
Article:
Bowie, A. orcid.org/0009-0008-6246-4544, Hitchcock, A. orcid.org/0000-0001-6572-434X, Proctor, M. orcid.org/0000-0002-1484-850X et al. (3 more authors) (2025) Cyanobacterial redox carriers support photosynthesis in a purple phototrophic bacterium. Biochemical Journal. BCJ20253114. ISSN 0264-6021

https://doi.org/10.1042/bcj20253114

Cyanobacterial redox carriers support photosynthesis in a purple phototrophic bacterium

Adam G.M. Bowie[1], Andrew Hitchcock[1,2*], Matthew S. Proctor[1], Elizabeth C. Martin[1], David J.K. Swainsbury[3] and C. Neil Hunter[1*]

[1]Plants, Photosynthesis and Soil, School of Biosciences, University of Sheffield, UK.

[2]Molecular Microbiology: Biochemistry to Disease, School of Biosciences, University of Sheffield, UK.

[3]School of Biological Sciences, University of East Anglia, Norwich Research Park, Norwich, UK.

*Correspondence: C. Neil Hunter (c.n.hunter@sheffield.ac.uk); Andrew Hitchcock (a.hitchcock@sheffield.ac.uk)

Author ORCID IDs: 0009-0008-6246-4544 (AGMB), 0000-0001-6572-434X (AH), 0000-0002-1484-850X (MSP), 0000-0001-9600-7298 (ECM), 0000-0002-0754-0363 (DJKS), 0000-0003-2533-9783 (CNH).

Abstract

In oxygenic and anoxygenic photosynthesis, excitation energy migrates from a surrounding antenna to specialised chlorophyll (Chl) or bacteriochlorophyll (BChl) pigments housed within a reaction centre (RC) complex. Here, a charge-separated state is formed within a few picoseconds, and an electron moves along a series of cofactors until it arrives at a quinone or iron-sulfur centre acceptor. Further photochemical cycles rely on rapid re-reduction of the photo-oxidised RC, usually by small, soluble metalloproteins which vary considerably between different phototrophic clades. In the purple phototrophic bacterium *Rhodobacter* (*Rba.*) *sphaeroides*, the electron carrier cytochrome c_2 (cyt c_2) shuttles between the periplasmic faces of the cytochrome bc_1 complex and the

reaction centre-light harvesting 1 (RC-LH1) core complex, the location of the BChl special pair (P_{865}). By contrast, in the model cyanobacterium *Synechocystis* sp. PCC 6803, electrons are transferred from cytochrome b_6f to photosystem I (PSI) via two isofunctional redox carrier proteins, cytochrome c_6 (cyt c_6) and plastocyanin (Pc). In this paper, we demonstrate that both cyt c_6 and Pc can substitute for cyt c_2 *in silico*, *in vitro* and *in vivo*, even though their electrostatic properties may be counter-productive for binding the RC-LH1 complex. Interestingly, whilst P_{865}^+ reduction was highest with cyt c_2 and the full physiological RC-LH1 complex, both *Synechocystis* proteins were more compatible with the RC-only complex lacking the surrounding LH1 antenna. Taken together, this suggests the subunits that constitute the LH1 ring improve both the donor side activity and selectivity of the *Rba. sphaeroides* RC complex.

Keywords: photosynthesis, RC-LH1, PSI, redox carrier proteins, *Rhodobacter sphaeroides*, *Synechocystis* sp. PCC 6803, electron transfer, cytochromes, plastocyanin

Subjects: Biophysics, Bioenergetics, Enzymology, Microbiology, Molecular Interactions, Photosynthesis, Synthetic Biology, Biochemical Techniques & Resources

Introduction

Oxygenic and anoxygenic photosynthesis are powered by spectrally distinct reaction centres (RCs) that share a common evolutionary origin [1-4]. This relatedness is evident from the structural homology between the five core transmembrane helices of all extant RCs, but after billions of years of divergent evolution, modern RC complexes share little meaningful sequence identity [2]. Some RCs use bacteriochlorophylls (BChls) as their primary charge-separating pigments whilst others harness chlorophylls (Chls), but their electron acceptors are the basis for delineating two RC classes. Following photochemical charge separation, Type I (Fe-S type) RCs pass electrons to iron-sulfur clusters via

either of the two pseudosymmetric branches of cofactors, then pass electrons to iron-sulfur clusters, whereas type II (Q-type) RCs reduce quinone acceptors via the active branch (A-branch) of cofactors [1]. There are also differences in the way electrons are supplied to the photooxidised primary pigments, resetting RCs for further rounds of photochemistry. The electron donors to both type I and type II RCs in the photooxidised state are generally small, mobile electron carriers such as *c*-type cytochromes or plastocyanin, with the notable exception of Photosystem II (PSII) in cyanobacteria, algae and plants, which has evolved the capacity to extract electrons from water, generating oxygen as a 'waste' by-product [5,6]. The green or purple phototrophic bacterial clades make either type I or type II RCs, respectively, and have relatively simple, cyclic photosynthetic electron transfer chains, whereas cyanobacteria, algae and plants evolved the ability to assemble both RC types, specifically Photosystem I (PSI) and the water-oxidising PSII complex [7]. Consequently, oxygenic photosynthesis employs a linear electron transfer pathway that couples PSII, cytochrome b_6f and PSI complexes so that electrons from water are eventually used to reduce CO_2 to simple carbohydrates [8].

Photosynthetic organisms occupy specific spectral niches related to the light-absorbing pigments they produce. Purple phototrophic bacteria synthesising BChl *a* harvest near-infra-red light in the 750-950 nm spectral region, whereas oxygenic phototrophs equipped with PSI and PSII use Chls to harvest visible light below 750 nm. This kind of specialisation has led to proposals to combine the attributes of both Chl- and BChl-containing RC complexes in a host organism, generating a hybrid, light-driven electron transfer system with an expanded spectral range able to absorb nearly all photosynthetically active solar radiation [9,10]. The native arrangement of the PSII and PSI complexes, which both bind Chl *a*, was suggested to be inherently inefficient because both photosystems compete for the same solar photons [9]. Their vision of reengineered photosynthesis replaced Chl *a*-containing PSI with a BChl *b*-based RC complex termed "RC1", creating a more efficient photochemical system

with complementary light absorption properties and minimal spectral overlap [9]. A subsequent proposal also replaced PSI with a BChl *b*-containing type II RC that drives an electron transfer loop involving the cytochrome b_6f complex, resembling cyclic electron transport in phototrophic bacteria. This new arrangement would generate a protonmotive force that drives the ATP synthase, whilst $NADP^+$ could be reduced by the NAD(P)H dehydrogenase complex (NDH-1) operating in reverse [10].

A more recent proposal [11,12], depicted in Figure 1, retains the native PSII and PSI photosystems whilst introducing a new BChl *a*-based type II RC complex termed PSIII, forming a three-photosystem hybrid array that can utilise the visible, red, far-red and near-infra-red regions of the solar spectrum. In this arrangement, intended to operate in a minimal cyanobacterial chassis [13], an engineered BChl-PSIII and the native Chl-PSI complex would compete for the same electron donors, cyt c_6 and Pc, with the relative electron flux through the two RCs being determined by whether the chromatic environment preferentially excites either Chl or BChl [11]. A minimally effective PSIII complex could be optimised by using adaptive laboratory evolution (ALE), which has already been used to introduce new traits in photosynthetic organisms such as high-light tolerance [14,15].

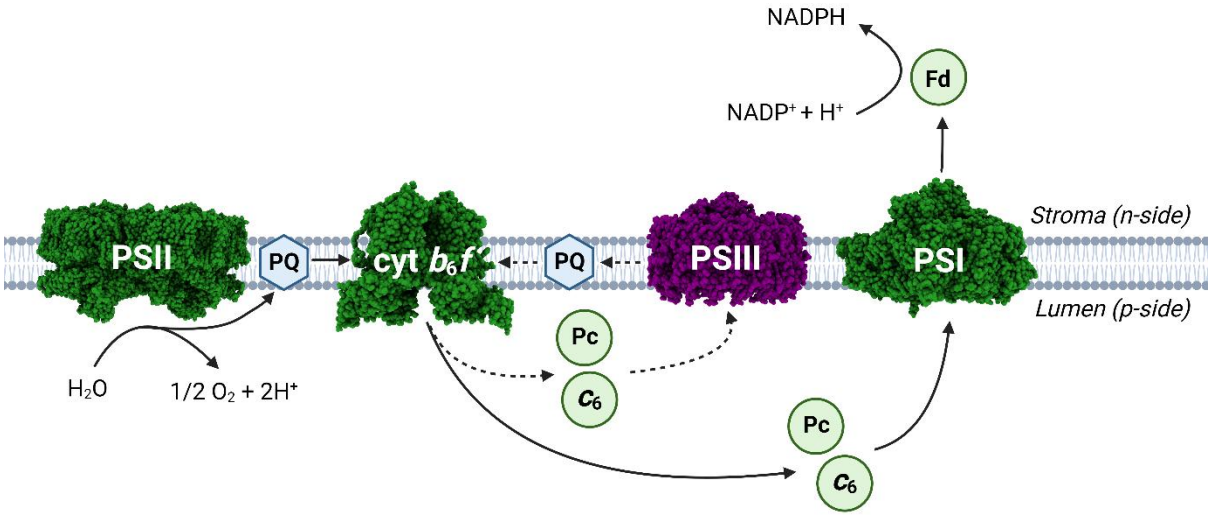

Figure 1: Envisaged Three-Photosystem Electron Transport Chain in a Transgenic Cyanobacterium

Electron transport pathways in a "photo-redesigned" thylakoid membrane, as proposed by Hitchcock et al. [11], with native electron transfer proteins depicted in green and a near-infrared absorbing third photosystem ("PSIII") based on RC-LH1 coloured purple. This heavily redesigned complex would oxidise cyt c_6/Pc and pass photoexcited electrons to plastoquinone, forming an additional cyclic electron transfer loop with cyt b_6f (dashed lines) that contributes to thylakoid lumen acidification and ATP production. Space-filling models are included for PSI [16], PSII [17], cyt b_6f [18] and RC-LH1 [19] structures, with LHC-type antennas and host cyclic electron transfer pathways omitted for clarity.

The list of modifications and genetic manipulations required to assemble a purple bacterial RC complex in a cyanobacterial chassis is formidable, particularly the heterologous expression of RC-LH1 structural genes alongside their assembly factors and the wholesale rewiring of pigment biosynthesis pathways to make both Chl and BChl simultaneously [11]. Using the well-characterised RC complex from *Rba. sphaeroides* as a starting point for PSIII, extensive protein engineering would also be required to make the complex compatible with the native cyanobacterial photosynthetic machinery, reducing plastoquinone (PQ) instead of ubiquinone (UQ) and oxidising cyt c_6 and Pc rather than cyt c_2. To investigate the feasibility of a PSIII complex, we have determined the level of pre-existing compatibility at the donor side of the *Rba. sphaeroides* RC complex for binding the native cyt c_2 relative to cyt c_6 and Pc counterparts from *Synechocystis* sp. PCC 6803.

PSI and RC-LH1 accept electrons from soluble redox carrier proteins at binding sites that can be divided into two regions with different properties. In both RC types a short-range interaction domain composed primarily of hydrophobic residues acts as the site of electron transfer, located on a pair of antiparallel helices that lie directly above the primary charge-separating pair of (B)Chls (named P_{865}) [3,20,21]. This region interacts with the face of the incoming

electron donor through a series of van der Waals (vdW) contacts, hydrogen bonds and cation-π interactions, which are centred around a functionally imperative aromatic electron tunnelling contact, Tyr-L162 in RC-LH1 [20,22,23], and a pair of π-stacked tryptophan residues in PSI [24-26]. By contrast, a long-range interaction domain is formed by more distal charged residues making a series of complementary electrostatic interactions that steer the redox carrier protein towards its target via a transient encounter complex [20,27,28]. The balance between these two domains is different in the two RC complexes. The PSI interface is simpler and more symmetrical, being dominated by hydrophobic interactions and two arginine-aspartate charge pairs, whilst the RC-LH1 binding site has a much larger electrostatic component, featuring a ring of amino acids with negatively charged side chains [20,28,29].

The compartmentalisation of hydrophobic and charged residues is also apparent in the structures of the redox carrier proteins. In the class I c-type cytochromes cyt c_2 and cyt c_6, uncharged residues border the leading edge of the heme c prosthetic group, whilst in the blue copper protein Pc a non-polar patch of residues known as the "northern face" surrounds His-86, a key amino acid known to be part of the electron transfer pathway to PSI [30-32]. An outer ring of positively charged residues in cyt c_2 makes electrostatic interactions with RC-LH1, whilst cyt c_6 and Pc have acidic patches for interactions with PSI [25, 32-34], although the eukaryotic homologs of these two proteins have much greater negative charge density due to electrostatic interactions with PsaF that are absent from cyanobacteria [25, 30, 35-37]. These differences in donor-acceptor binding interfaces between PSI, RC-LH1, and their respective electron donors should present a significant obstacle to cross-species compatibility, even though the RCs and their respective cytochrome redox carriers share significant structural homology. Here, we investigate the capacity of cyt c_6 and Pc to replace cyt c_2 as the electron donor to RC-LH1 and RC complexes *in silico*, *in vitro* and *in vivo*. We show that cyt c_6 is an adequate replacement for the native cyt c_2 donor *in vivo* despite its intrinsically low RC reduction rate *in vitro*,

whilst Pc is a uniformly poor electron donor to RCs in both situations. However, the *in vivo* performance of Pc can be greatly improved by ALE, which has the effect of raising heterologous Pc synthesis at least four-fold. We also identify possible roles for the additional subunits that surround the RC core complex, including the LH1 αβ polypeptides, PufX, protein-Y and protein-Z. Although it is not known which subunits are responsible, the presence of these LH1-associated proteins collectively improves both the activity of the RC complex and its electron donor selectivity.

Results

Cyt c_6 and Pc productively bind RC-LH1 in AlphaFold3 Predicted Complexes

Once bound together in a complex, the rate of electron transfer between two redox-active proteins is determined by a range of highly sensitive parameters, including the difference in midpoint redox potentials that determines the driving force (ΔG), the reorganisation energy (λ) and the edge-to-edge distance between two redox active cofactors [38]. Whilst RC-donor systems can tolerate significant changes in ΔG values [39], nearly all productive biological electron transfers occur over a narrow distance range of 4-14 Å, making the binding location and orientation of an incoming redox carrier protein functionally imperative [40].

Despite billions of years of divergent evolution, both cyt c_6 and Pc are predicted by AlphaFold3 [41] to bind the *Rba. sphaeroides* RC in the same position as the co-evolved cyt c_2, with their redox-active cofactors positioned less than 14 Å of the special pair in the predicted co-structures (Figure 2). This was also the case for isocytochrome c_2 (iso c_2), a redundant second genomically-encoded donor to RC-LH1 which is upregulated in "spd" suppressor mutants of *Rba. sphaeroides* when the *cycA* gene for cyt c_2 is knocked out [42]. Since the midpoint redox potentials of cyt c_6 (+324 mV) and Pc (+360 mV) [43] are very similar to cyt c_2 (+352 mV) [44] and iso c_2 (+294 mV) [45], we predicted that all four redox carrier proteins would be capable of reducing P_{865}^+ once bound. The predicted structures also suggest cyt c_6 and Pc have some affinity for the cyt c_2 binding site on the RC, which is corroborated by protein-protein docking simulations of AlphaFold2-predicted complexes in the HADDOCK 2.4 server [46,47]. In these simulations, the two *Synechocystis* proteins are predicted to make similarly strong vdW interactions with RC-LH1 compared to cyt c_2, but the electrostatic forces were significantly weaker (Supplementary Figure 1), in keeping with their lower surface charge densities (Figure 3). Calculations suggest the electron transfer rate from Pc is likely to be several orders of magnitude slower than for the cytochromes (Supplementary Table 2), not least because the donor and acceptor cofactors are 13.1 Å apart, the longest of the distances in Figure 2 [20, 40, 41, 43, 44, 45, 48-50].

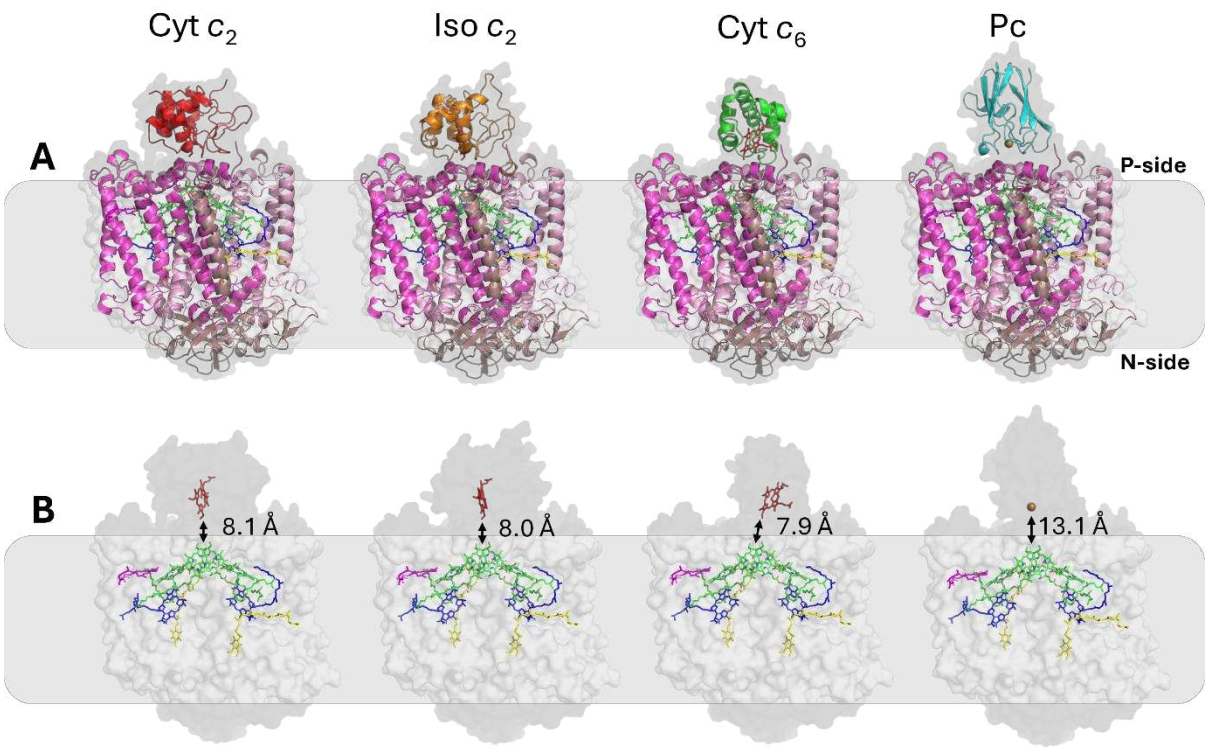

210

211 **Figure 2. AlphaFold3-predicted complexes of the *Rba. sphaeroides* RC with**
212 **native and non-native redox carrier proteins.**

213 **(A)** Cartoon representations of the RC-L (pink), RC-M (magenta) and RC-H
214 (brown) core subunits bound to cyt c_2 (red), iso c_2 (orange), cyt c_6 (green) and
215 Pc (cyan). **(B)** Transparent space-filling models of the complexes, with cofactors
216 visible including heme (red), copper (orange), BChl (green), bacteriopheophytin
217 (blue) and ubiquinone (yellow). Distances are labelled, with the predicted edge-
218 to-edge distances between the heme *c* in cyt c_2 and the primary pair BChls
219 being only slightly lower than the 8.4 Å value determined by X-ray
220 crystallography [20].

221

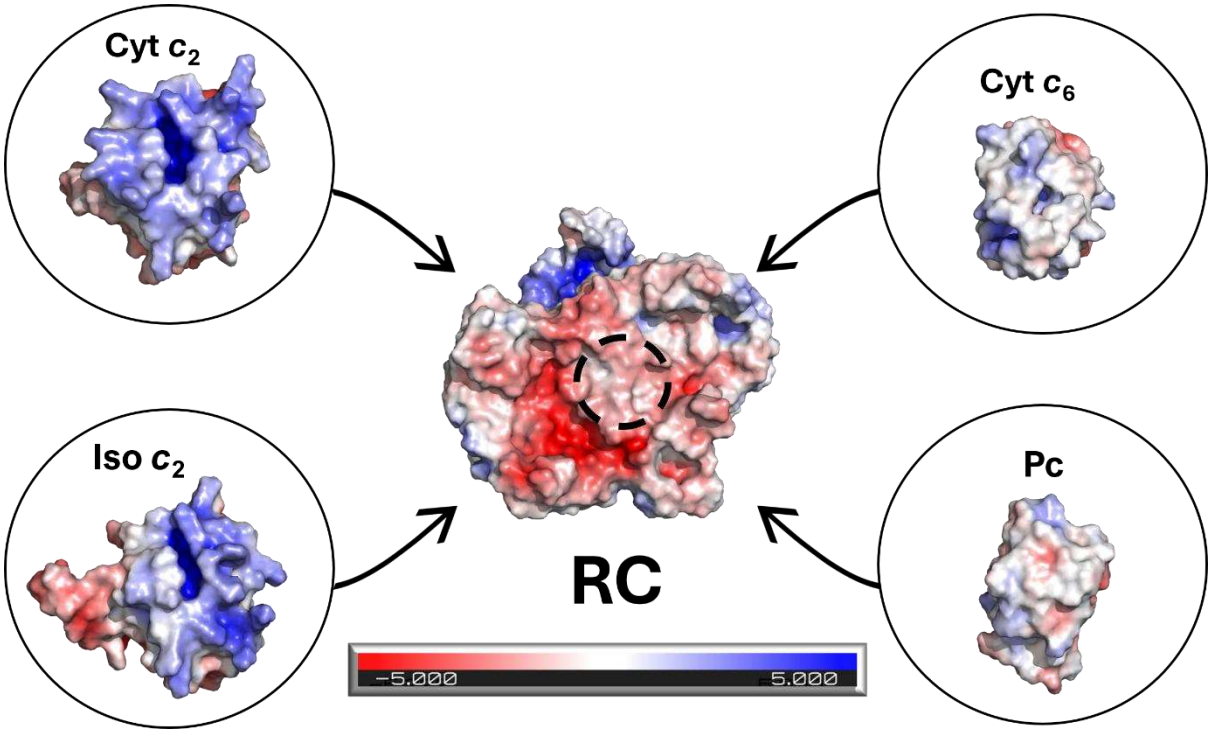

Figure 3. Surface electrostatics of the *Rba. sphaeroides* RC and various soluble electron donors.

Surface charges on the binding faces of selected electron transfer proteins in 'open book' style, showing the periplasmic face of the RC and the incoming faces of the four electron donors (circled) that dock onto the RC. Structures were generated using AlphaFold2 [51], visualised in PyMol and coloured using the APBS plugin [52], with negative charges in red, positive charges in blue and uncharged patches in white, with colour strength denoting charge density.

Both cyt c_6 and Pc can substitute for cyt c_2 *in vivo*

To determine how closely computational predictions correspond to *in vivo* behaviour, a photosynthetically incompetent Δ*cycA* Δ*cycI* strain of *Rba. sphaeroides* was constructed which lacked both endogenous redox carrier proteins that can support photosynthetic growth [42,53]. Plasmid-borne genes encoding the four different electron donor proteins were transferred to the Δ*cycA* Δ*cycI* strain, generating four transconjugant strains carrying *cycA* (cyt c_2), *cycI* (iso c_2), *petJ* (cyt c_6) or *petE* (Pc). In each transconjugant strain, redox carrier genes were placed under the transcriptional control of a constitutively active promoter, $Ppuf_{843-1200}$, in the broad-host replicative vector pBBRBB [54]. Using a consistent starting inoculum of semi-aerobically grown cells, transconjugants were cultured photoheterotrophically under 24 µmol m^{-2} s^{-1} illumination alongside positive wild type (WT) and negative Δ*cycA* Δ*cycI* control strains carrying empty pBBRBB plasmids. The resulting 48-hour growth curves and doubling times presented in Figure 4 demonstrate the very similar growth rates of the WT (empty pBBRBB) control and the *cycA* transconjugant strain (Δ*cycA* Δ*cycI*::pBBRBB *cycA*), whereas the *cycI* (iso c_2) transconjugant strain (Δ*cycA* Δ*cycI*::pBBRBB *cycI*) grows slightly more slowly, possibly due to the 40-fold lower affinity iso c_2 has for the RC relative to cyt c_2 [55]. The growth curve for Δ*cycA* Δ*cycI*::pBBRBB *petJ* shows that cyanobacterial cyt c_6 is sufficiently compatible with RC-LH1, cytochrome bc_1 and the host metabolic machinery to restore a near-WT photoheterotrophic growth rate to the *Rba. sphaeroides* Δ*cycA* Δ*cycI* mutant (Figure 4A). By contrast, the *petE* transconjugants were barely viable, with doubling times over 10-fold longer than the WT (Figure 4B). However, after approximately 10 days of minimal growth, the photosynthetic growth rate of the three *petE* transconjugant cultures suddenly increased 5-fold (Figure 5A), possibly arising from a growth-enabling suppressor mutation [56-58]. This shorter doubling time was maintained when the suppressor strains were isolated and then cultured photoheterotrophically for a second time, with *petE* transconjugants growing only ~3.1 times more slowly than the WT control and without a lag phase (Figure 5A). Relative quantification of redox carrier proteins in the periplasm

using sodium deoxycholate (see Materials and Methods) revealed that, unlike cyt c_6, the bioavailability of Pc in *petE* transconjugants is initially very poor, and that the mechanistic basis of improved growth is a dramatic improvement in intracellular Pc levels without any changes to the plasmid sequence or knockout loci (Figure 5B). Despite having a mean periplasmic redox carrier concentration 1.7 times higher than in *petJ* transconjugants ($p < 0.05$), the fact the growth rate of the evolved *petE* transconjugants remained almost three-fold slower is further evidence that RC-LH1 and cyt bc_1 are much more compatible with cyt c_6 than Pc under physiological conditions, assuming all redox carriers are incorporated equally within chromatophore vesicles. Although different methods were used to quantify cytochrome and Pc levels, Figure 5B shows that the amount of Pc accumulated in the periplasm of the evolved *petE* transconjugant strains was twice that of cyt c_2 in the WT strain ($p < 0.01$) and over 7 times more than the original *petE* transconjugants before ALE occurred ($p < 0.001$).

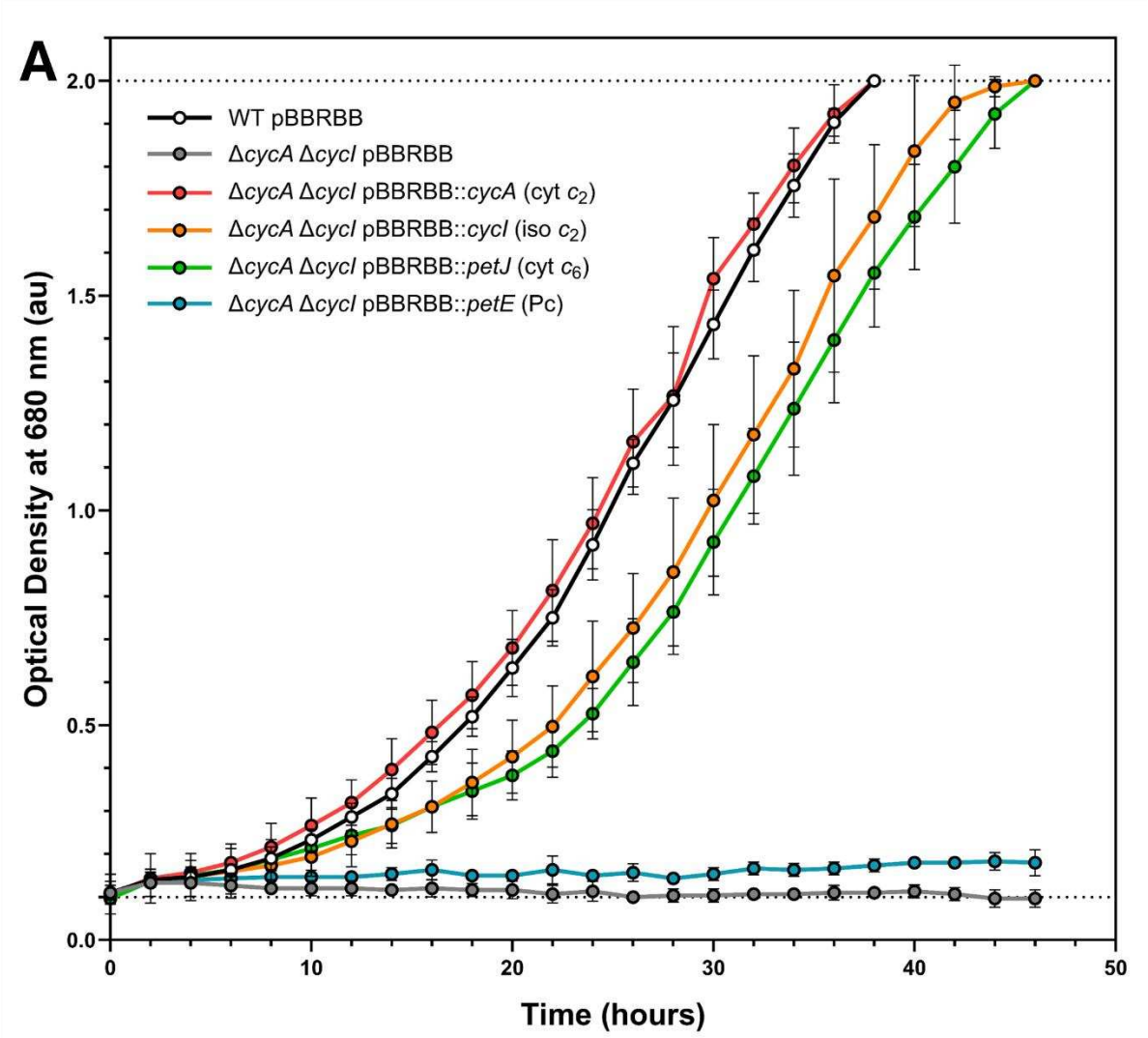

B

Transconjugant Strain	Rate Constant (*k*)	Doubling Time (hours)
WT pBBRBB	0.074	9.42
ΔcycA ΔcycI pBBRBB	-0.005	-
ΔcycA ΔcycI pBBRBB::*cycA*	0.076	9.15
ΔcycA ΔcycI pBBRBB::*cycI*	0.072	9.69
ΔcycA ΔcycI pBBRBB::*petJ*	0.067	10.3
ΔcycA ΔcycI pBBRBB::*petE*	0.007	103

Figure 4. Photoheterophic growth curves of *Rba. sphaeroides* strains with native and non-native redox carriers

(**A**) Cultures were grown in triplicate and measured at 2-hour intervals. Dotted lines at Y = 0.1 and Y = 2 represent the starting OD_{680} values and detection limit, respectively. (**B**) Table of growth rate parameters colour coded according to the data in panel (**A**). In panel (**A**) and all subsequent instances, the error

bars displayed are +/- one standard deviation from the mean and n=3 unless otherwise stated.

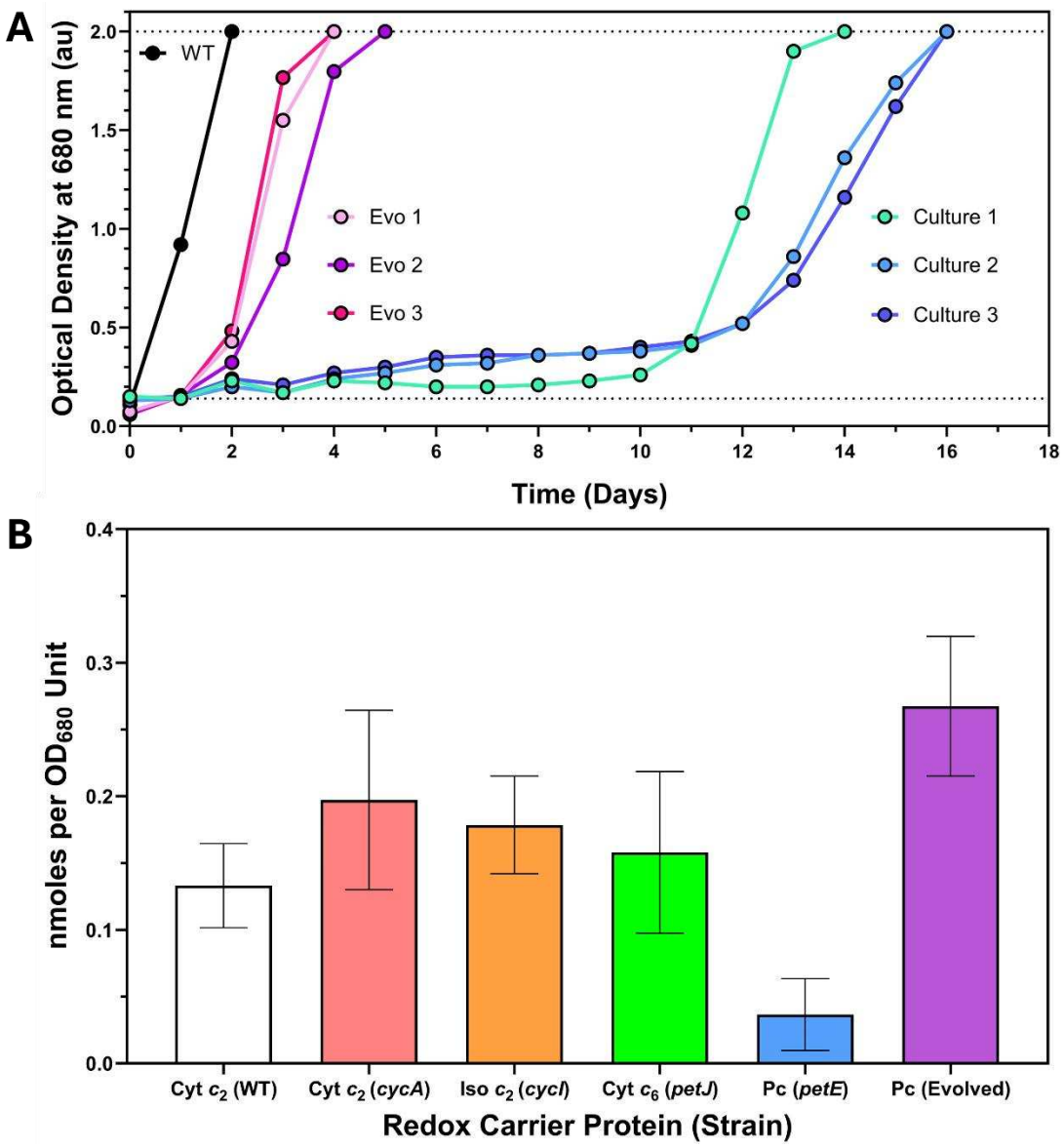

Figure 5. Photoheterotrophic growth curves of *petE* transconjugants and relative periplasmic concentrations of redox carrier proteins in all transconjugant strains.

(A) Extended photoheterotrophic growth curves comparing WT pBBRBB (positive control, black) to individual *petE* transconjugant cultures (genotype Δ*cycA* Δ*cycI* pBBRBB::*petE*, blue shades). Cells from each *petE* culture were harvested, streaked to single colonies on M22 agar and grown semi-aerobically to make 3 evolved strains (Evo 1, Evo 2 and Evo 3), with each number corresponding to the culture number from which the cells were isolated. These Evo strains were then grown photoheterotrophically under the same conditions as the original set of growth curves, with the resulting data superimposed onto

the 16-day growth curves (pink shades). The average doubling time of the evolved *petE* transconjugants in the second growth experiment was 28.6 hours with a rate constant of 0.0243, approximately 5 times faster than in the first growth experiment. **(B)** The relative amounts of each redox carrier protein that could be extracted from the periplasm of each transconjugant strain using sodium deoxycholate (see materials and methods). Three biological replicates were conducted for all proteins, except for Pc in the evolved strains (purple), for which n = 9.

RC-LH1 displays very low compatibility with cyt c_6 and Pc in steady-state turnover assays conducted under low ionic strength

Whilst the behaviour of different redox carriers *in vivo* is a complex function of their affinity for RC-LH1, the cytochrome bc_1 complex and the host's wider metabolism, *in vitro* steady-state turnover assays allow direct measurement of the compatibility of the four redox carrier proteins with the RC-LH1 complex. 300 µl reaction mixtures were made containing a fixed 0.125 µM concentration of RC-LH1, 50 µM ubiquinone-2 (UQ-2, a soluble analogue of the native ubiquinone-10 substrate with a shorted isoprenoid tail) and a ≥ 20-fold excess of one of the pre-reduced redox carrier proteins, each of which was purified from the periplasm using a novel technique involving sodium deoxycholate (see Materials and Methods). In each assay, RC turnover was initiated by continuous illumination with an 810 nm LED and the oxidation of reduced donors monitored by measuring absorbance at their respective redox-sensitive wavelengths. These reactions were conducted in triplicate under the optimum *in vitro* conditions for the RC-LH1-cyt c_2 system (50 mM Tris-HCl at pH 7.5 with 100 mM NaCl and 0.03 % (w/v) β-DDM) as determined by separate steady-state turnover experiments (See next section and Supplementary Figure 2). To act as a benchmark for turnover rates, the performance of cytochrome *c* from horse heart mitochondria (cyt *c*) was also measured, since this commercially available protein has been used extensively as an effective *in vitro* analogue of cyt c_2 in historical RC literature despite sharing just 32.7 % identity [59,60]. A titration series was conducted for each redox

carrier protein and the initial rates of oxidation used to construct Michaelis-Menten plots, from which V_{max} and K_M values could be calculated (Figure 6).

The Michaelis-Menten plots in Figure 6A-C display a clear disparity between the native redox carrier proteins from *Rba. sphaeroides* and their counterparts from *Synechocystis*, with a compatibility order matching the *in vivo* growth curves and the HADDOCK 2.4 predicted affinities. Under the assay conditions there was little difference in the V_{max} and K_M values for cyt c_2, iso c_2 and cyt *c*, which all lie within error of each other, but the oxidation rates of cyt c_6 and Pc are much slower than the *in vivo* results would suggest (Figure 6D). This indicates that whilst cyt c_6 and Pc can reduce P_{865}^+ fast enough *in vivo* to support photoheterotrophic growth, their intrinsic level of compatibility with the RC-LH1 complex is very low outside of the confined chromatophore environment.

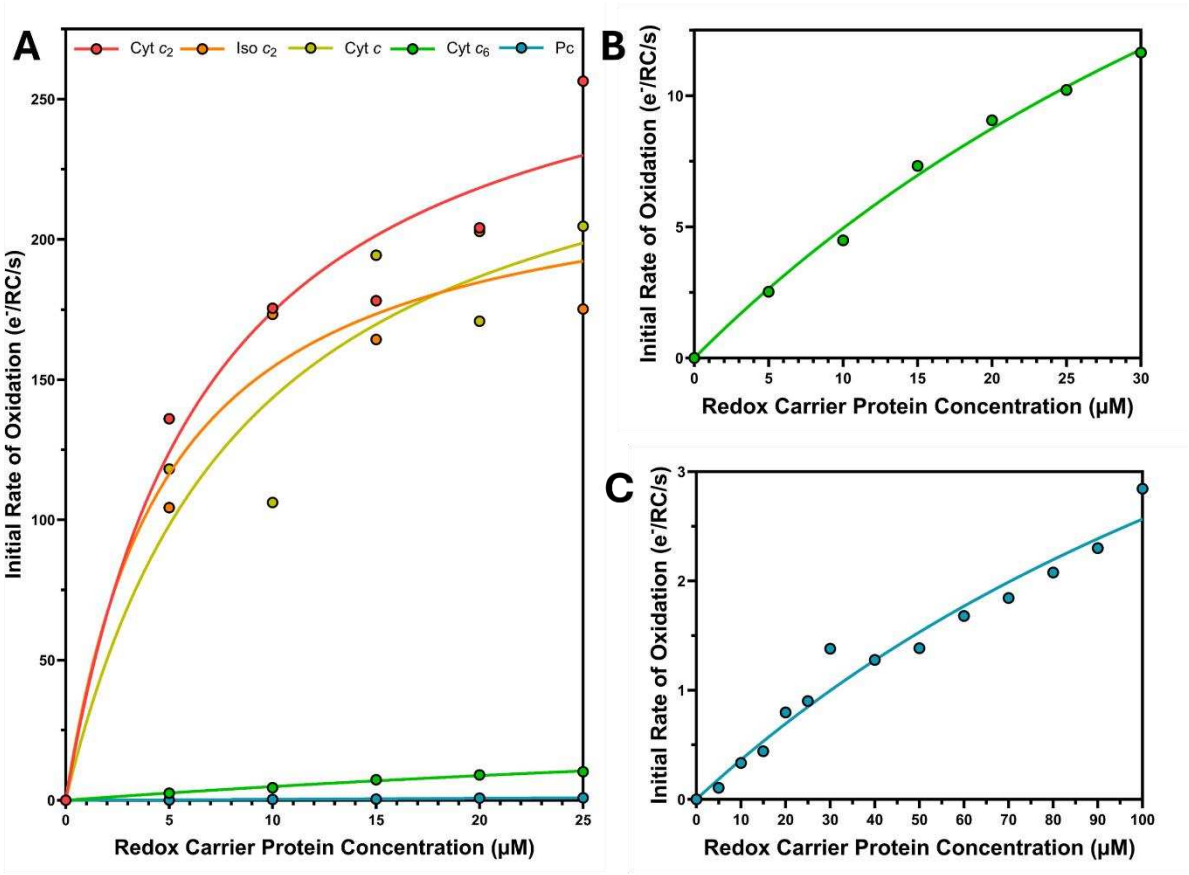

D

Redox Carrier Protein	V_{max} (e^-/RC/s) (Best Estimate)	V_{max} (e^-/RC/s) (95 % CI)	K_M (μM) (Best Estimate)	K_M (μM) (95 % CI)	R Squared
Cyt c_2	293	218 – 473	6.80	1.89 – 21.2	0.833
Iso c_2	230	189 – 293	5.88	1.94 – 10.3	0.890
Cyt c	267	190 – 469	8.63	2.49 – 27.9	0.837
Cyt c_6	37.8	25.5 – 77.1	66.3	37.80– 160	0.975
Pc	7.92	5.42 – 15.8	209	121 – 488	0.951

Figure 6. Michaelis-Menten plots, including V_{max} and K_M estimates for oxidation of different redox carriers by RC-LH1 complexes.

(A) Michaelis-Menten plots of redox carrier oxidation rate at 25 °C against the concentration of cyt c_2 (red), iso c_2 (orange), cyt c (yellow), cyt c_6 (green) and Pc (blue). **(B)** Expanded Michaelis-Menten plot of redox carrier oxidation rate versus cyt c_6 concentration. **(C)** Expanded Michaelis-Menten plot of redox carrier oxidation rate versus Pc concentration. **(D)** Estimates for V_{max} and K_M, along with the 95 % confidence intervals for both parameters and the coefficient of determination (R-squared) demonstrating the goodness of fit to the Michaelis-Menten equation used to determine the two parameters in GraphPad Prism 10 (Domatics). 1 mM ascorbate was included in the reaction mixtures of cyt c_2, iso c_2 and cyt c to keep each donor reduced before the light-

359 on time. However, this reagent was omitted from reaction mixtures containing
360 cyt c_6 or Pc as these proteins remained reduced during dark adaption and
361 ascorbate addition was found to lower their oxidation rates and amplitudes.

362

Redox Carrier Proteins from *Rba. sphaeroides* and *Synechocystis* display opposite salinity trends in their interactions with RC-LH1

Whilst there is a clear oxidation rate hierarchy for the different redox carriers, the conditions used to collect the data in Figure 6 are unlikely to reflect the physiological conditions within chromatophores and may selectively favour the oxidation of the two native redox carriers by RC-LH1. To determine the optimum NaCl concentrations for the oxidation of the five different redox carrier proteins by RC-LH1, steady-state turnover assays were conducted at pH 7.5 with 0.25 μM RC-LH1 and a fixed 80-fold excess of redox carrier protein, along with 50 μM UQ-2, 0.03 % (w/v) β-DDM and 1 mM ascorbate for cyt c_2, iso c_2 and cyt c, with NaCl added at 25 or 100 mM intervals.

Plotting oxidation rate against salinity, as shown in Figure 7A, 7B, reveals decidedly different behavioural trends between the two groups of redox carrier proteins with RC-LH1; whilst the oxidation rates of cyt c_2, iso c_2 and cyt c are highest between 25 and 100 mM NaCl, the optimum NaCl concentrations for cyt c_6 and Pc are much higher, lying between 600 and 800 mM. These dramatically increased, and nearly identical, optimum salt concentrations for cyt c_6 and Pc may be a consequence of incompatible electrostatic interactions with RC-LH1 that are screened at high salinities. Amongst the three redox carrier proteins that perform better under lower salinities, it is perhaps unsurprising that the physiological RC-LH1 electron donor, cyt c_2, has both the highest optimum NaCl concentration and is the least affected by salt-screening, with the RC-LH1-cyt c_2 system retaining about 40 % of its maximum activity at 500 mM NaCl (Figure 7C). By contrast, the interaction between RC-LH1 and cyt c is more easily disrupted by salinity, having lost 90 % of its cyt c oxidation activity by 500 mM (Figure 7C), with an observed 50 mM optimum NaCl concentration comparable with the 40 mM value found previously for the antenna-free RC-cyt c system (Figure 7A) [60]. The decline in iso c_2 oxidation rate is intermediate between cyt c_2 and cyt c, with only 20 % of maximum activity remaining at 500 mM, revealing a clear order of electrostatic complementarity where cyt c_2 makes the most specific and high affinity interactions with RC-LH1. A consequence of this differential salt dependency is

395 that at much higher salt concentrations the gap in RC-LH1 reduction activity
396 between the native and *Synechocystis* redox carriers is significantly lower
397 (Figure 7C), although the compatibility of Pc remains poor.

398

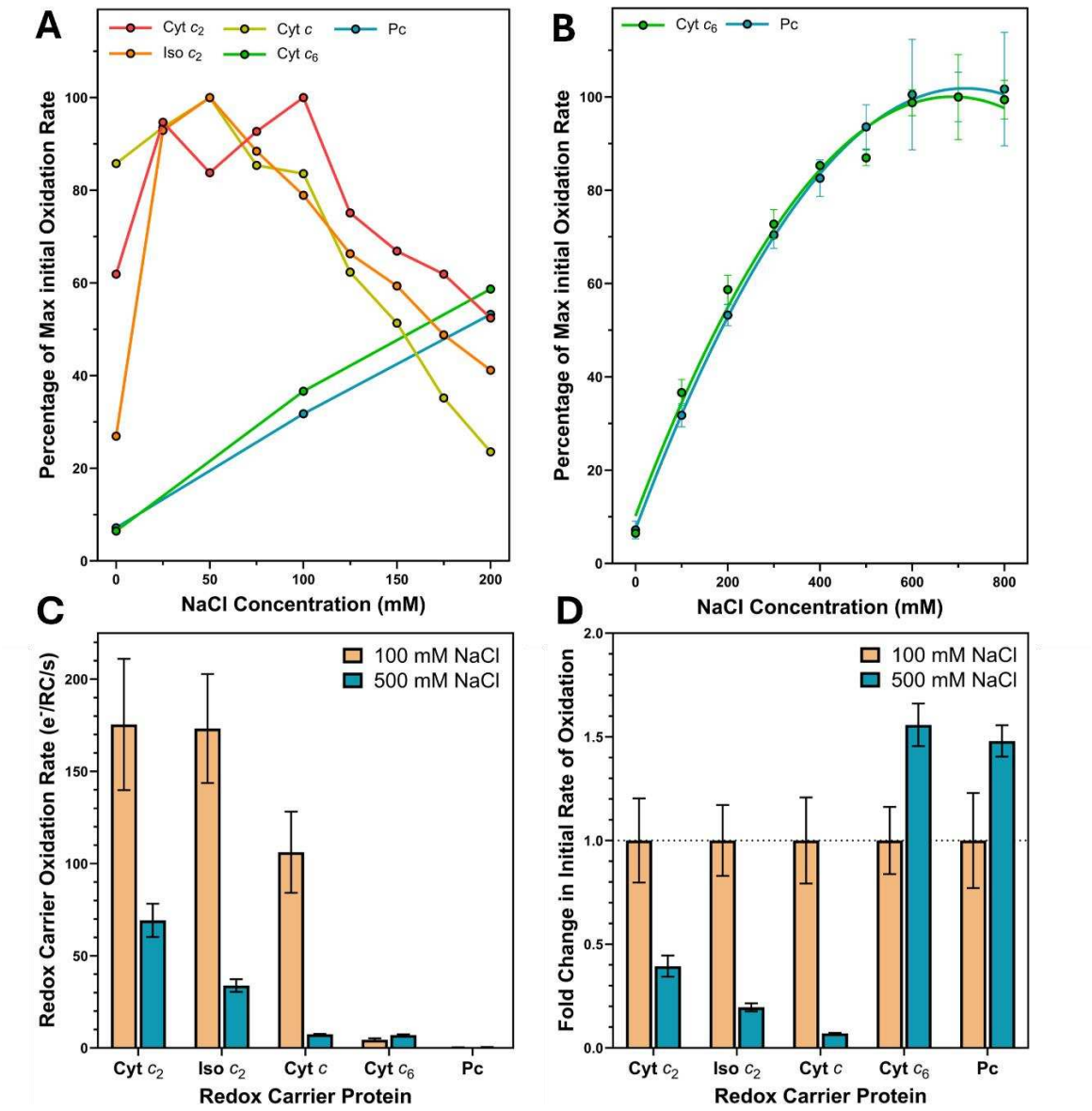

Figure 7. Effect of increasing NaCl Concentration on initial rates of redox carrier oxidation by RC-LH1 Complexes

Salt dependency of the interactions between RC-LH1 with **(A)** class I cytochromes between 0 and 200 mM NaCl and **(B)** Pc and cyt c_6 between 0 and 800 mM NaCl. All reactions were carried out in triplicate and normalised to each redox carrier protein's maximum rate and thus the graphs show the percentage change in activity with increasing salinity. Error bars are omitted from panel **(A)** for ease of viewing, with just the mean values plotted for each salt concentration, whilst in panel **(B)** the data are fitted to a centred second order polynomial (quadratic) function, with R-squared values of 0.98 for both

cyt c_6 and Pc. **(C)** Raw initial rates of redox carrier oxidation by RC-LH1 under low salinity (100 mM NaCl, orange) and high salinity (500 mM NaCl, blue). **(D)** Fold change in initial rates of redox carrier oxidation by RC-LH1 from 100 mM (orange) to 500 mM NaCl (blue). All reactions were carried out at 25 °C, with each 300 µl reaction mixture containing 0.25 µM RC-LH1, 10 µM redox carrier protein, 50 µM UQ-2, 50 mM Tris-HCl at pH 7.5 and 1 mM ascorbate for cyt c_2, iso c_2 and cyt c. Error bars are omitted for clarity in panel **(A)** Raw oxidation rates for the data in panel **(A)** and **(B)** can be found in Supplementary Figure 3.

LH1 ring subunits modulate both acceptor and donor side electron transfer activity

Since the first RC purification by Reed and Clayton in 1968 [61], it has been common practice to solubilise *Rba. sphaeroides* membranes in detergents such as Triton X-100 or lauryldimethylamine oxide (LDAO) which removes LH1 -associated subunits (mainly LH1 α, β, but also X, Y and Z), leaving the more experimentally accessible RC-only complex. In steady-state turnover assays this truncated complex, which consists of just the three core RC subunits L, M and H, behaves very differently to the physiological RC-LH1 system under its optimal conditions (50 mM Tris at pH 7.5, 100 mM NaCl). Not only is the cyt c_2 oxidation rate by the RC-only complex more than 30 % slower than for RC-LH1 (Figure 8A, 8B), but it also appears to be salt concentration independent under the conditions of this steady-state assay (Figure 8C). Since only the solvent-exposed cyt c_2-binding site (donor side) of the complex is affected by salt, this result suggests the activity of the RC-only complex is held back by Q_B turnover, making it acceptor side limited. This theory is corroborated by an observed increase in cyt c_2 oxidation rate by RC-only complexes when decyl-ubiquinone (DUQ, Sigma) was exchanged for UQ-2, a ubiquinone analogue with a more physiological tail composed of 2 isoprene units rather than a saturated decane chain, whilst no difference in behaviour was observed between these two analogues with RC-LH1 (Figure 8D). This phenotype was found to be highly robust and repeatable, being observed consistently across many technical and biological repeats, including when RC-only complexes were purified from LH1-

minus ΔpufBA strains or directly from photosynthetically grown RC-LH1 complexes containing spheroidene by LDAO treatment (data not shown). Follow-up steady state turnover experiments also confirmed that this difference in quinone analogue sensitivity between the two forms of the RC complex cannot be explained by the additional light-harvesting capacity of the LH1 ring, since under the conditions of the assay the RC-only complex is already light-saturated (Supplementary Figure 4).

Along with responding differently to salinity, cyt c_6 and Pc also display opposite trends to cyt c_2 with the truncated RC-only complex (Figure 8A,8B). Whilst the initial oxidation rates of cyt c_2, iso c_2 and cyt *c* are all improved ~1.5-fold by switching from the RC-only to the RC-LH1 version of the complex, the opposite is true for cyt c_6 and Pc, whose oxidation rates drop 3-fold. This suggests there is a fundamental incompatibility between the *Synechocystis* redox carrier proteins and the LH1-associated subunits that surround the RC core complex. Collectively, these subunits appear to not only confer higher acceptor side activity by improving quinone reduction but also seem to impart greater donor side selectivity by hindering the binding of non-cognate proteins that lack the correct properties. The LH1 ring may also promote cyt c_2 binding through electrostatic steering, as suggested in our recent single molecule force spectroscopy study [28], which could also contribute to the observed difference in cyt c_2 oxidation rates between RC-only and RC-LH1 complexes.

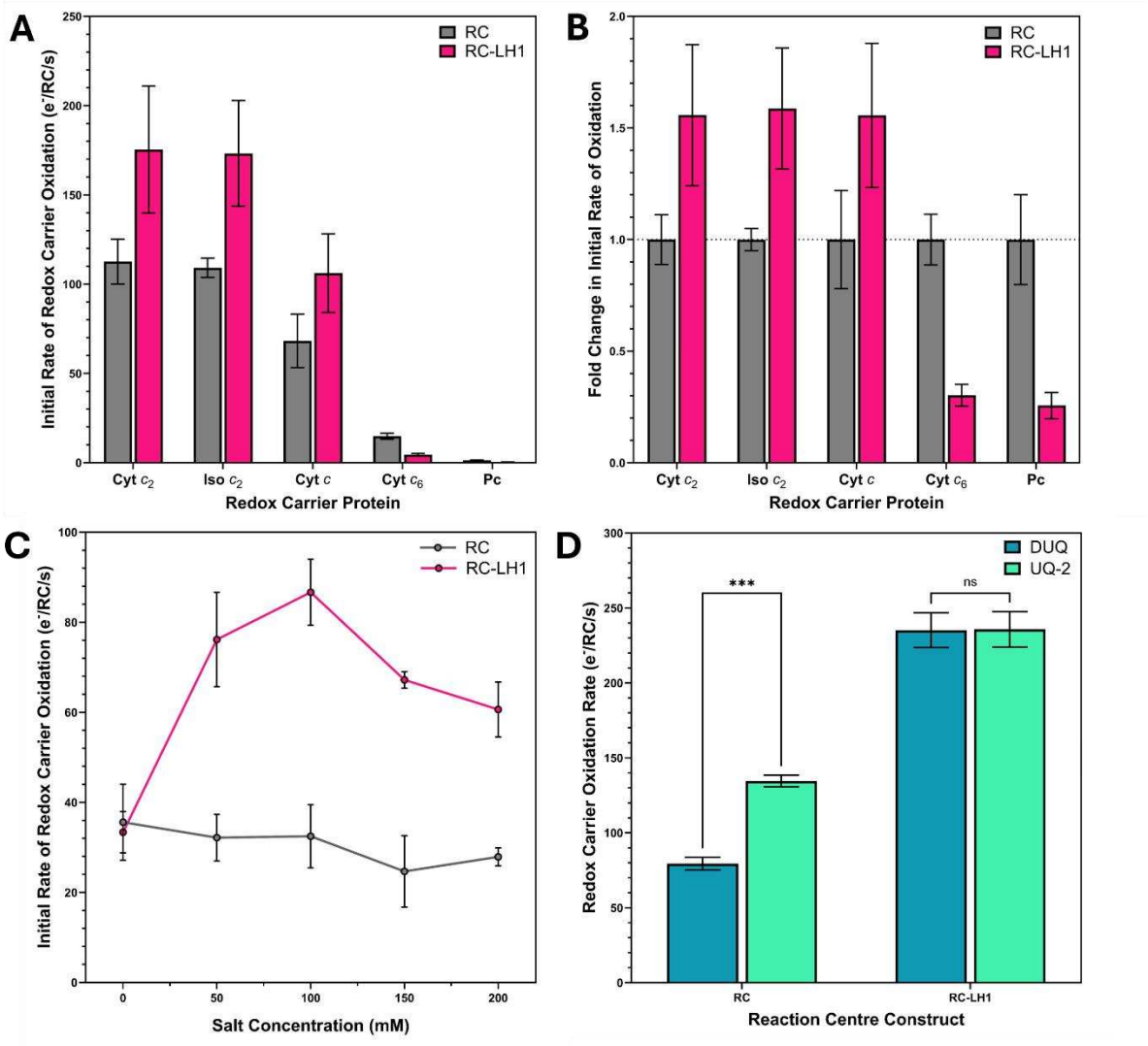

Figure 8. Kinetic behaviour of RC-only and RC-LH1 complexes under different conditions

(A) Raw initial rates of redox carrier oxidation during steady-state turnover assays by RC-LH1 (pink) and RC-only complexes (grey). Assays were conducted at 25 °C in 50 mM Tris-HCl pH 7.5 and 0.03 % (w/v) β-DDM, with 0.125 μM RC or RC-LH1, 10 μM redox carrier, 50 μM UQ-2 and 1 mM sodium D-ascorbate. **(B)** Fold change in RC-LH1 initial oxidation rates compared to RC-only for each redox carrier protein, from the dataset plotted in **(A)**. **(C)** Initial rates of cyt c_2 oxidation by RC-LH1 (pink) and RC-only complexes (grey) in response to increasing [NaCl], with conditions of 0.5 μM RC/RC-LH1, 10 μM cyt c_2 and 0.03 % (w/v) β-DDM in 50 mM Tris-HCl pH 8, along with 1 mM ascorbate for reaction mixtures containing RC-LH1 but not RC-only complexes.

(D) Bar chart comparison of initial rates of cyt c_2 oxidation by RC-LH1 and RC-only complexes with two different quinone analogues, decyl ubiquinone (DUQ, blue) and ubiquinone-2 (UQ-2, cyan). Reactions were carried out with 0.5 μM RC/RC-LH1, 11 μM cyt c_2, 0.5 mM ascorbate and 50 μM DUQ/UQ-2, with a p value of < 0.001 (***) for the RC-only complex with the two different analogues, calculated from an unpaired t-test using the Holm-Šídák method to account for multiple comparisons.

Discussion

The data presented in this paper demonstrate that despite billions of years of divergent evolution, the *Rba. sphaeroides* RC-LH1 complex displays a surprisingly high level of *in vivo* compatibility for the cyanobacterial cyt c_6 and Pc redox carriers from *Synechocystis* sp. PCC 6803, which usually reduce PSI. Although both *Synechocystis* proteins can shuttle electrons between the RC-LH1 and cytochrome bc_1 complexes efficiently enough to support photoheterotrophic growth *in vivo*, *in vitro* and *in silico* data paint a more complex picture of compatibility compared to the two native redox carrier proteins in *Rba. sphaeroides*. Computational modelling predictions, photoheterotrophic growth rates and steady-state turnover assays all converge on a predicted RC-LH1 compatibility order where cyt c_2 is the best electron donor to P_{865}, followed by iso c_2, then cyt c_6 and finally Pc, but different methods give different relative estimates due to fundamental differences in behaviour between these redox carrier proteins. Whilst cyt c_2 and iso c_2 were oxidised fastest by RC-LH1 at low salinities (50 – 100 mM NaCl), the fastest turnover rates for cyt c_6 and Pc were achieved with the RC-only complex and high salinities (600 - 750 mM). A third non-native redox carrier, cyt *c* from *Equus caballus*, showed the same trends as the *Rba. sphaeroides* redox carriers, but its performance compared to the native *Rba. sphaeroides* cyt c_2 fell away sharply with increased salinity. Taking all these data together, several key differences emerge between the RC-LH1-cyt c_2 and PSI-cyt c_6/Pc systems, as well as some unexpected properties of the RC-LH1 complex. Although Pc is intrinsically much less compatible with RC-LH1, likely because it hails from a different family of proteins, the identical behavioural trends exhibited by cyt c_6 and Pc are in keeping with their isofunctional roles in thylakoid electron transfer [62,63]. Regardless of the nature of their interaction, it may be that any reduced redox carrier protein with a suitable redox potential can reduce P_{865}^{+} if its redox-active cofactor can be positioned within 14 Å of the special pair.

The rate at which different redox carrier proteins can reduce the RC-LH1 complex in the steady state is a function of three countervailing processes, binding (k_{on}), electron transfer (k_{ET}) and unbinding (k_{off}), all of which require a range of different parameters to be maintained within a narrow range. Protein-protein docking in AlphaFold3 and HADDOCK 2.4 suggest that both cyt c_6 and Pc bind RC-LH1 in sufficient proximity and in the correct orientation to support productive electron transfer (Figure 2) (Supplementary Figure 1), but their different surface properties are a barrier for binding to the RC (Figure 3). Whilst both long-range electrostatic steering and short-range hydrophobic interactions are important for binding both PSI and RC-LH1, the binding partners in *Rba. sphaeroides* have a much greater electrostatic force component, whilst cyt c_6 and Pc have much lower surface charge densities (Figure 2). As a result of these differences, it may be that the PSI cyt c_6/Pc binding interface is intrinsically weaker than RC-LH1-cyt c_2/iso c_2, especially since the experimentally determined K_D for plant PSI-Pc [64] is 70 times greater than RC-cyt c_2 [65].

Given the predicted lower affinities of cyt c_6 and Pc for binding RC-LH1, it follows that their oxidation rates are much lower than for cyt c_2 but, perhaps surprisingly, they operate better at much higher salinities albeit still at low absolute rates. Since electron transfer rates from cyt *c* to P_{865}^+ are off-rate limited below the optimum salt concentration and on-rate limited above this value [60], it seems likely that a very slow k_{on} is limiting at low salinities, which we speculate could be linked to counter-productive electrostatic interactions between the highly negatively charged surface of the RC-LH1 complex (Figure 9A) and the two *Synechocystis* redox carriers. These interactions may be repulsive, pushing cyt c_6 and Pc away from the site of electron transfer, or may steer the two proteins into the wrong orientation for binding, where the correct face of the redox carrier is pointed away from the periplasmic surface of the RC-LH1 complex. This would explain why improved oxidation rates for cyt c_6

and Pc are recorded when salt screening of charges increases or when the LH1 ring is removed from the complex.

Taken together, the differential effects of salt screening and subunit composition on the redox carrier proteins also suggest that the subunits which surround the RC core complex are required not just for light harvesting, but also for maximising the activity and selectivity of electron donors under optimal conditions. If the surface charges on each LH1 αβ pair can be unfavourable for the binding of cyt c_6 and Pc, then it is likely that the opposite can be true for the native RC-LH1 electron donor, with molecular dynamics data suggesting the LH1 ring has a degree of affinity for cyt c_2 [28]. It is therefore possible that LH1 αβ pair electrostatics are partially responsible for the observed rate difference in cyt c_2 oxidation between RC-only and RC-LH1 complexes, with possible roles for surface charges in recruitment, orientation, entrance and exit pathways for redox carrier proteins (Figure 9B). However, this difference can also be explained by an acceptor side limitation in the truncated three-subunit RC-only complex, which is supported by the sensitivity of its turnover rate to different quinone analogues. The way that RC-LH1 complexes are donor-side limited under the same conditions and do not respond to quinone analogue changes suggest the LH1 α and β polypeptides that surround the RC, along with the X, Y and Z subunits, act in concert to increase acceptor side quinone turnover. The mechanism by which these subunits enhance acceptor side turnover could involve providing efficient entrance and exit channels, providing a "conveyor belt" pathway for quinones to rapidly enter the Q_B binding site and leave as soon as they are doubly reduced [66,67]. Additional low-affinity ubiquinone binding sites, which might act as a "waiting room" to increase the local concentration of incoming quinones, have already been identified in cryo-EM structures of the *Rhodopseudomonas palustris* RC-LH1 complex and involve π-stacking interactions between tryptophan residues and quinone head groups [66,68], whilst π-stacking and hydrogen bonding with side chains on LH1 αβ subunits have also been implicated in quinol exit pathways [67]. In the *Rba.*

sphaeroides RC-LH1 complex, accessory entrance and exit sites might be found in the transmembrane helices of the αβ pairs, or might even be associated with the X, Y and Z subunits which are already known to maintain open quinone channels to the membrane, completing a "highway" for quinone diffusion between RC-LH1 and cytochrome bc_1 [53, 68-72].

Ultimately however, under almost all light levels, the activity of the RC-LH1 complex is not limiting for photosynthetic growth; the slowest step in the cyclic purple bacterial electron transport chain is widely acknowledged to be quinol oxidation by the cytochrome bc_1 complex instead [73-75]. This means that a non-native redox carrier protein substituting for cyt c_2 would not limit photosynthetic growth rate if it oxidised cytochrome bc_1 and reduced RC-LH1 more rapidly than the cytochrome bc_1 complex can oxidise ubiquinol. For *petJ* and *petE* transconjugant strains growing photoheterotrophically (Figure 3), a slower rate of RC-LH1 re-reduction could be tolerated with only a slight increase in doubling time, masking the true difference in compatibility between the native redox carrier proteins and their counterparts from *Synechocystis*. This could explain why, following ALE of *petE* transconjugants by a currently unknown mechanism, the compatibility of cyt c_6 and Pc unusually appears higher *in vivo* than *in vitro*, rather than the other way around.

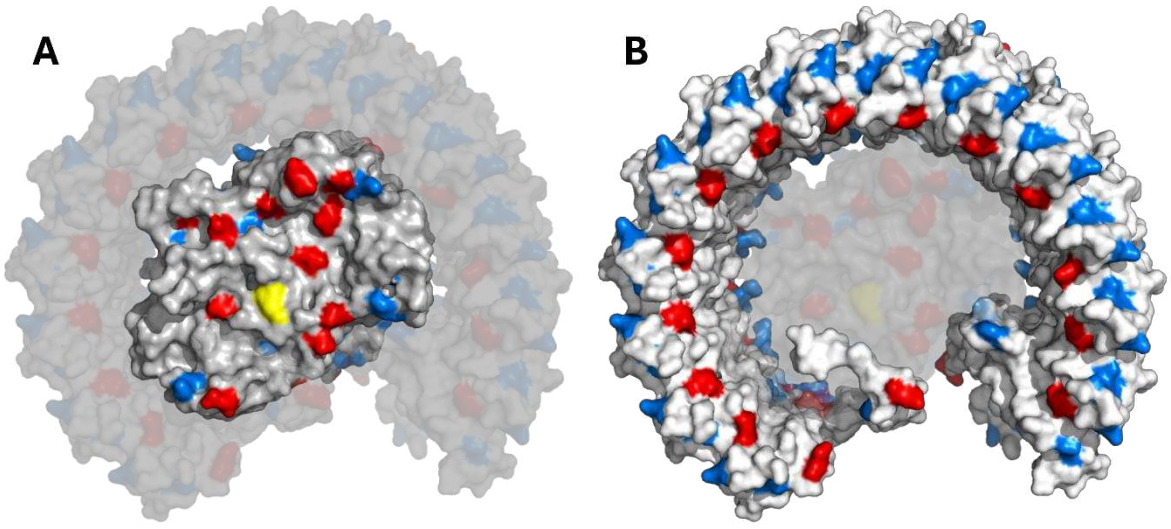

Figure 9. Comparison of surface electrostatics on the periplasmic faces of the RC and LH1 components of the RC-LH1 complex

(A) Surface representation of the periplasmic faces of the RC-L and RC-M subunits with other subunits set to 65 % transparency, whilst **(B)** shows the periplasmic face of the rest of the complex, including all ring subunits (α, β, X, Y and Z chains), with RC-L and RC-M set to 65 % transparency. In both **(A)** and **(B)**, amino acids with negatively charged side chains are coloured red, with positively charged residues in blue and Tyr-L162 shown in yellow to mark the site of electron transfer. Structure shown in this figure is the RC-LH1 monomer complex from [19], PDB 7PIL.

The differences between *in vivo* and *in vitro* data summarised in Table 1 can also be reconciled in the context of the conditions of the chromatophore lumen, which will almost certainly have a pH, viscosity and salinity that differ from laboratory conditions whilst also containing different types of salts and solutes, plus a lipid bilayer. The conditions inside a chromatophore vesicle cannot be replicated *in vitro* and in this tiny compartment, which has a typical internal diameter of just 45 nm [76], K_D and K_M values are rendered irrelevant by the effective redox carrier concentration within the chromatophore lumen, which for cyt c_2 is estimated to be 600 μM [74], a value 3 orders of magnitude greater than the K_D value of 0.3 μM for the RC-cyt c_2 system [65]. The periplasmic concentrations for cyt c_6 and Pc in the ALE strains are comparable to that for cyt c_2 (Figure 5B), and therefore still exceed the measured K_M values of 66 and 209 μM, respectively. Thus, *in vivo* compartmentalisation of reactants can overcome apparent *in vitro* limitations, and in this case, excess amounts of cyt c_6 and Pc are already capable of productively shuttling electrons between RC-LH1 and cytochrome bc_1, raising the prospects that synthetic biology can bring together photosynthetic proteins that evolution has long since separated.

Table 1. Summary of experiments conducted with host and *Synechocystis* redox carrier proteins

	Cyt c_2	Iso c_2	Cyt c_6	Pc
Edge-to-Edge Distance (Å)	8.1	8.0	7.9	13.1
HADDOCK Score	-183	-144	-104	-91.9
Predicted k_{et} (s^{-1})	1.38×10^9	7.53×10^9	3.23×10^9	2.77×10^5

Doubling Time (hours)	9.15	9.69	10.3	36.1
V_{max} (e^-/RC/s)	293	230	37.8	7.92
K_M (µM)	6.80	5.88	66.3	209
Optimum [NaCl] (mM)	100	50	700	700

629

630

631

Materials & Methods

Generation of strains and plasmids

The work described in this paper was carried out in several strains of *Rba. sphaeroides* 2.4.1, along with *E. coli* strains for molecular cloning and conjugative transfer of plasmids, all of which are listed in Table 2. For complementation studies and protein production, an unmarked genomic deletion strain lacking the endogenous photosynthetic redox carrier genes (genotype Δ*cycA* Δ*cycI*) was generated using the pK18mobsacB system as previously described [53]. The DX13 and E9 strains lacking various RC-LH1 and LH2 genes were generated by sequential rounds of pK18mobsacB mutagenesis following the protocol detailed in [77]. Unmodified genes encoding cyt c_2 (*cycA*), iso c_2 (*cycI*), cyt c_6 (*petJ*) and Pc (*petE*) were PCR amplified from their host organism using primers listed in Supplementary Table 1, digested with BglII and XhoI/SalI (Thermo Fisher Scientific), then ligated into the broad-host range vector pBBRBBB-$Ppuf_{843-1200}$ [54]. Following sequence verification by Sanger sequencing (Eurofins genomics), the resulting plasmids were transformed into *E. coli* S17-1 and conjugated into the Δ*cycA* Δ*cycI* strain of *Rba. sphaeroides*, using 30 μg ml^{-1} kanamycin to select transconjugants. A similar strategy was employed for the RC subunit-encoding *pufLM* genes, with PCR fragments being cloned into the same vector at the BglII/SpeI restriction sites, conjugation of the ligated plasmid into the E9 (Δ*puc1BA* Δ*pufBALM*) strain. A *petE*-StrepII-tag insert was also made by PCR from *Synechocystis* sp. PCC 6803 cells and cloned into a pET28a vector using NcoI and XhoI restriction sites, then transformed into the *E. coli* BL21(DE3) strain (Promega) for Strep-tagged Pc production.

Table 2. Bacterial strains used in this study

Species/strain	Genotype	Properties	Source/Reference
***Rhodobacter sphaeroides* 2.4.1**			
Wild type	N/A	Wild type strain	S. Kaplan (University of Texas)

ΔcycA Δcycl	ΔcycA Δcycl	Unmarked deletion of *cycA* (RSP_0296) and *cycI* (RSP_2577); does not produce cyt c_2 (*cycA*) or iso c_2 (*cycI*)	[53]
DX13	Δ*puc1BA* Δ*puc2BA* PufX R49L R53L	Unmarked deletion strain of LH2 genes, *puc1BA* (RSP_0314-0315) and *puc2BA* (RSP_1556-1557). Replacement of arginine residues in PufX responsible for dimerization with leucine so strain exclusively makes RC-LH1 monomers.	This study S. Kaplan (University of Texas) (Δ*puc1BA*) [78] (Δ*puc2BA*) [79] (PufX R49L R53L)
E9	Δ*puc1BA* Δ*pufBALM*	Unmarked deletion strain of LH2 genes, *puc1BA* (RSP_0314-0315), along with *pufBALM* (RSP_6108, RSP_0258-0256) encoding the RC-LH1 l, M, α and β subunits.	This study S. Kaplan (University of Texas) (Δ*puc1BA*)
Escherichia coli			
BL21(DE3)	F−*ompT hsd*SB (r_B^-, m_B^-) *gal dcm* (DE3)	Protein production strain	Promega
JM109	*end*A1, *rec*A1, *gyr*A96, *thi*, *hsd*R17 (r_k^-, m_k^+), *rel*A1, *sup*E44, Δ(*lac-proAB*), [F′ *tra*D36, *pro*AB,	Cloning strain	Promega

	lacI^{q}ZΔM15]		
S17-1	RP4-2 (Tc::Mu, Nm::Tn7) integrated into the chromosome *Tp*^{R} *Sm*^{R} *recA*, *thi*, *pro*, *hsdM*$^{+}$	Conjugative transfer of plasmids to *Rba. sphaeroides*	[80]
Synechocystis	**sp. PCC 6803**		
Wild type	N/A	Glucose-tolerant wild-type strain	R. Sobotka (Algatech, Třeboň)

658

659 **Semi-aerobic growth of *Rba. sphaeroides* cells**

660 *Rba. sphaeroides* cells were cultured in M22+ medium [81]. Kanamycin (30 μg
661 ml^{-1}) was added to maintain plasmids where necessary. Three different types of
662 flat-bottomed glassware were used to make liquid cultures. In the first liquid
663 culture step, universal tubes containing 10 ml of medium (about 25 % full) were
664 inoculated with single colonies from M22 agar plates and grown at 30 °C with
665 shaking at 150 rpm until pigmented (~24-48 h). A single 10 ml culture was
666 then used to inoculate either 80 ml medium in a 125 ml Erlenmeyer flask and
667 grown overnight, or 1.6 l medium in a 2 L conical flask and grown for 72 h.
668 The universal tubes were sealed with a screw top cap; the other cultures were
669 kept sterile with a cotton wool bung topped with two layers of aluminium foil.

670 **Photoheterotrophic growth of *Rba. sphaeroides* cells**

671 Anoxic conditions promoting photoheterotrophic growth were achieved by fully
672 filling and stoppering glassware with M22+ medium. Larger cultures for RC-
673 LH1 purification were grown in 1 l Roux bottles stoppered with a rubber bung
674 whilst for growth curves, narrow ~18 ml glass tubes were inoculated with cells
675 from semi-aerobic 80 ml cultures, using the OD_{680} value to estimate culture
676 turbidity and calculate the amount of inoculum needed to ensure a consistent
677 starting cell density of ~0.1. Cultures were illuminated by a 70 W Halogen

Classic Bulbs (Phillips) usually at 25 µmol m^{-2} s^{-1} and agitated with magnetic stirrers until reaching stationary phase, which corresponds to an approximate OD_{680} of 3. Growth curve culture turbidity at 680 nm was measured with a CO7500 Colorwave colorimeter (WPA). The doubling times of photoheterotrophic cultures were calculated by non-linear fitting in GraphPad Prism 10 using the exponential (Malthusian) growth function.

Purification of intracytoplasmic membranes

All RC-LH1 complexes were purified as monomers from DX13 cells (Δ*puc1BA* Δ*puc2BA* PufX R49L R53L) grown photoheterotrophically in a 1 l Roux culture bottle as described above. Cells were harvested at 4,200 x*g* for 30 minutes at 4 °C and the resulting pellets resuspended in 50 mM Tris-HCl pH 8 supplemented with an EDTA-free protease inhibitor tablet (Merck) to a total volume of 30 ml. Resuspended cells were incubated at room temperature with lysozyme for 20 minutes, before DNase I was added and the cells placed on ice. Cells were lysed by two passages through a chilled French press at 124 MPa and the lysate was clarified by centrifugation at 27,000 ×*g* for 20 min at 4 °C to remove cell debris. Intracytoplasmic membranes (ICM) were prepared by layering clarified supernatant on top of a 15/40 % (w/v) discontinuous sucrose gradient, then centrifuged at 84,500 ×*g* for 10 h at 4 °C. The pigmented band of ICM formed at the interface was harvested with a serological pipette and centrifuged again at 185,500 ×*g* for 2 h at 4 °C.

Purification of RC-LH1 complexes

Pelleted ICM were resuspended in 50 mM Tris-HCl pH 8 and homogenised before being solubilised in 2 % (w/v) β-DDM. RC-LH1 complexes were purified by a round of anion exchange on a 150 ml DEAE Sepharose column at 5 ml min^{-1}, using a gradient of 200 -300 mM NaCl in 20 mM Tris-HCl pH8 with 0.03 % (w/v) β-DDM. After spin concentration using 100 kDa molecular weight cut-off (MWCO) concentrators (Thermo Fisher), gel filtration chromatography was carried out on a HiLoad® 16/600 Superdex® 200 pg column (Cytiva) in 50 mM Tris-HCl pH 8 with 200 mM NaCl and 0.03 % (w/v) β-DDM at a flow rate of 0.5 ml min^{-1}.

Purification of RC-only complexes

RC-only complexes containing spheroidenone were purified from E9 pBBRBB-$Ppuf_{843-1200}$ :: *pufLM* transconjugants grown semi-aerobically as described earlier. Cells were pelleted and lysed as described earlier but, rather than preparing ICM, membranes were harvested from clarified lysate by ultracentrifugation at 185,500 xg for 2 h at 4 °C in a type 45 Ti ultracentrifuge rotor (Beckman) and transferred to a small Duran bottle containing 100 ml 50 mM Tris-HCl pH 8. These membranes were resuspended and solubilised at room temperature by stirring in the presence of 1 % (v/v) LDAO, deliberately harsh conditions to remove other membrane proteins in the mixture. After loading onto a homemade 150 ml DEAE Sepharose column, RCs were purified by anion exchange in 20 mM Tris-HCl pH 8 with 0.1% (v/v) LDAO using a 160-240 mM NaCl gradient, and a 5 ml min^{-1} flow rate on an ÄKTA Prime FPLC (Cytiva). Purified eluate was spin concentrated to <0.5 ml with 50 kDa MWCO centrifugal concentrators (Sartorius) then purified further by gel filtration at 0.5 ml min^{-1} on a HiLoad® 16/600 Superdex® 200 pg column (Cytiva) into 50 mM Tris-HCl pH 7.5, with 100 mM NaCl and 0.03 % (w/v) β-DDM.

RCs containing spheroidene must be purified from RC-LH1 complexes (see above) from anaerobic, phototrophically grown strains, by harnessing the sensitivity of LH1 αβ subunit pairs to LDAO treatment. RC-LH1 complexes were buffer exchanged into 50 mM Tris-HCl buffer at pH 8 with 0.1 % (v/v) LDAO and loaded onto a 5 ml Q Sepharose column (Cytiva). Bound complexes were then washed with at least 10 column volumes of the same buffer with 4 % (v/v) LDAO, before RC-only complexes were eluted using 20 mM Tris-HCl at pH 8 with 0.1 % (v/v) LDAO and a 200 – 400 mM NaCl gradient at a flow rate of 5 ml min^{-1}.

Purification of c-type cytochromes from *Rba. sphaeroides*

All three untagged cytochromes (cyt c_2, iso c_2 and cyt c_6) could be purified from their respective transconjugant strains by first performing a novel deoxycholate-based fractionation technique, which efficiently separates the

contents of the periplasm from the bulk of the cellular proteome. Although the downstream purification steps varied between the four proteins, the periplasmic extraction process was the same each time. 1.6 l semi-aerobic cultures were pelleted at 4,200 ×*g* for 30 minutes at 4 °C and resuspended in ~20 ml periplasmic extraction buffer to a total volume of 40 ml, supplemented with EDTA-free protease inhibitor (Merck). This buffer, which was carefully designed to avoid whole cell lysis and deoxycholate hydrogel formation (McNeel et al., 2015), contained 100 mM HEPES at pH 8 for the two *Rba. sphaeroides* proteins or 100 mM CHES at pH 9 for cyt c_6, along with 500 mM sucrose and 50 mM NaCl as osmotic stabilisers. 0.8 g solid sodium deoxycholate were added to each cell suspension to make a 2 % (w/v) solution, which was then incubated in the dark at 4 °C with mild agitation. After an hour, spheroplasts were pelleted at 35,000 x*g* for 30 minutes at 4 °C and the supernatant, which contains the contents of the periplasm, taken forward to the next step (see below for specific details for each protein). Once purified, each redox carrier protein was concentrated to 2.5 ml in 3 kDa MWCO spin concentrators (ThermoFisher), reduced with sodium dithionite (Sigma) and buffer exchanged into the desired buffer using PD-10 desalting columns (Cytiva) according to the manufacturer's instructions.

Purification of untagged cyt c_2

Harnessing the propensity of divalent cations to precipitate bile acids, deoxycholate was removed from the periplasmic fraction by the addition of 6.25 ml 5 x deoxycholate precipitation solution (1 M ammonium acetate at pH 5 and 250 mM $MgSO_4$), mixing by inverting the tube and centrifugation at 35,000 x*g* for 30 minutes at 4 °C. The resulting supernatant was then passed through a homemade 30 ml SP Sepharose cation exchange column equilibrated in 50 mM ammonium acetate buffer at pH 5. Any red coloured eluate was collected, passed through a 0.22 µm filter, diluted 2.5-fold in 50 mM ammonium acetate at pH 5 and clarified by centrifugation at 15,000 x*g* for 10 minutes at 4 °C whilst the column was washed with successive column volumes of 1 M NaCl, 1 M NaOH and 100 % ethanol. The SP Sepharose was then re-equilibrated in 50 mM ammonium acetate at pH 5 and the clarified

coloured eluate loaded onto the column for a second time, resulting in binding of the target protein. Pure cyt c_2 could then be eluted over a gradient of 60 – 160 mM NaCl at 5 ml min^{-1} (Supplementary Figure 5).

Purification of untagged iso c_2

With its similar electrostatic properties, untagged iso c_2 was purified using the same column and buffer system used for cyt c_2. Following an identical deoxycholate precipitation step and centrifugation, clarified iso c_2 supernatant was passed through a 0.22 µm filter (Sartorius), diluted 10-fold with 50 mM ammonium acetate buffer at pH 5 and loaded directly onto the column. Cation exchange was performed to elute pure isocyt c_2 over a 150 – 250 mM NaCl gradient at 5 ml min^{-1} (Supplementary Figure 5).

Purification of untagged cyt c_6

The much lower surface charge density of the *Synechocystis* redox carrier proteins necessitated a different purification strategy. Instead of adding precipitation buffer, the periplasmic fraction containing cyt c_6 was clarified a second time at 35,000 ×*g* for 30 minutes, then passed through a 0.22 µm filter (Sartorius) and concentrated to ~10 ml in a 3 kDa MWCO spin concentrator (ThermoFisher). The concentrated cytochrome solution was then loaded onto a Hiprep 26/60 Sephacryl S-200 HR column (Cytiva) equilibrated in 50 mM CHES at pH 9 with 200 mM NaCl and run at 1.3 ml min^{-1}, taking 5 ml fractions. Any red/pink fractions were pooled and diluted 10-fold in 50 mM Tris pH 9, then loaded onto a 30 ml Q Sepharose column equilibrated in the same buffer. Anion exchange was then performed to purify cyt c_6 further, using a 30–80 mM NaCl gradient and a flow rate of 5 ml min^{-1} (Supplementary Figure 5).

Purification of Pc from *Rba. sphaeroides*

With the lowest affinity for ion exchange columns, Pc was the most challenging and time-consuming redox carrier to purify from *Rba. sphaeroides*. The redox carrier protein could only be purified from 1.6 l cultures of evolved *petE* transconjugant strains, by first lysing the cells by French press as described

earlier. Clarified lysate was then concentrated to ~2 ml in a 3 kDa MWCO spin concentrator (Sartorius) and oxidised by addition of a few grains of potassium ferricyanide. The 2 ml of oxidised cell lysate were then loaded onto a HiLoad® 16/600 Superdex® 200 pg gel filtration column (Cytiva) equilibrated in salt-free 50 mM Tris-HCl pH 9. As this column was run at 0.5 ml min^{-1} a blue Pc band became visible, along with red and yellow bands. All blue fractions were collected, pooled and diluted 10-fold in salt-free 50 mM Tris-HCl buffer pH 9, then loaded onto a 30 ml Q Sepharose column for anion exchange over a 25–75 mM NaCl gradient, collecting 5 ml fractions in tubes each containing a small amount of ferricyanide. Once Pc-containing fractions were spectrally identified, pooled and concentrated, a second gel filtration chromatography step was necessary to obtain the desired level of purity, using a Superdex® 75 10/300 GL column (Cytiva) with a running buffer containing 50 mM Tris-HCl pH 8 with 1 M NaCl and a flow rate of 0.3 ml min^{-1}. Untagged Pc was required to verify the full activity of a Strep-tagged isoform from *E. coli* which could be produced in higher yields (see below).

Purification of StrepII-tagged Pc from *E. coli*

To produce enough Pc for kinetic studies, we purified recombinant C-terminally StrepII-tagged Pc produced in *E coli*. 1 l of *E. coli* BL21(DE3) cells transformed with pET28a::*petE*-StrepII were grown at 37 °C in a baffled flask with 180 rpm agitation. When the OD_{600} reached 0.6, *petE* expression was induced by adding IPTG to 0.5 mM, along with $CuSO_4$ to a final concentration of 600 µM. Induced cells were incubated at 37 °C overnight with 180 rpm agitation and harvested the next day at 4,000 ×*g* for 30 minutes at 4 °C, then resuspended in 80 ml 20 mM Tris-HCl pH 7.4 with 250 mM DNAse I and 2 tablets of EDTA-free protease inhibitor added. Sodium deoxycholate was then added to a final concentration of 0.1 % (w/v) and the cell suspension mixed by magnetic stirring for 1 hour at room temperature before spheroplasts were removed by centrifugation at 8,000 ×*g* for 15 minutes at 4 °C. The supernatant was retained and after addition of several grains of potassium ferricyanide, the periplasmic fraction turned blue and was applied to a 4 ml Strep-Tactin XT 4Flow column (IBA life sciences). The column was washed with 20 mM Tris-HCl

pH 7.4, and pure Pc eluted with a column volume of the same buffer with 50 mM Biotin (Supplementary Figure 5). No statistically significant difference in turnover rate was found between untagged and Strep-tagged Pc in steady-state turnover assays with RC complexes (Supplementary Figure 6).

Determination of periplasmic protein concentrations, to assess the relative production levels for periplasmic cytochromes and blue copper proteins

Single colonies were grown to the 80 ml (see methods above) stage under semi-aerobic conditions and the entire culture was pelleted at 4,200 ×*g* for 30 minutes at 4 °C, removing the supernatant. Each pellet was then resuspended in 500 µl periplasmic extraction buffer (100 mM HEPES pH 8, 500 mM sucrose and 50 mM NaCl) from a 10 ml stock supplemented with 1 EDTA-free protease inhibitor tablet (Merck). The turbidity of each cell suspension was determined by performing a 200-fold dilution and measuring absorbance at 680 nm. Cells were diluted with periplasmic extraction buffer to make a 1 ml suspension for each strain with a consistent OD_{680} value. 200 µl of a 12 % (w/v) sodium deoxycholate stock solution in periplasmic extraction buffer were added to each 1 ml suspension and the tubes incubated in the dark with gentle agitation for 1 hour. Spheroplasts were pelleted in 1.5 ml Eppendorf tubes at 16,000 ×*g* for 30 minutes at 4 °C and 800 µl of each supernatant were transferred to a fresh tube. To remove the deoxycholate from solution, 200 µl 5 × deoxycholate precipitation solution (1 M ammonium acetate at pH 5 and 250 mM $MgSO_4$) was added to each 800 µl aliquot and mixed thoroughly by inverting the tubes. Most of the precipitated deoxycholate was removed from solution by centrifugation at 16,000 x*g* for 1 hour at 4 °C whilst 10 mM stocks of sodium dithionite and potassium ferricyanide were prepared in distilled water. After the centrifugation step, solutions were prepared containing each clarified periplasmic fraction and either 1 mM sodium dithionite or potassium ferricyanide in a 700 µl volume and centrifuged again in Eppendorf tubes at 16,000 x*g* for 3 hours at 4 °C.

The concentration of each redox carrier was determined by spectrophotometry in identical cuvettes using a Cary 60 spectrophotometer (Agilent Technologies) baselined to the extracted periplasm of the negative control strain (Δ*cycA*

Δ*cyc1* pBBRBB). Periplasmic extracts were prepared from two 80 ml cultures of this double knockout strain to provide a baseline for transconjugant strains making cytochromes or Pc. For cytochromes, the extract was reduced by sodium dithionite, whilst the second extract was oxidised with potassium ferricyanide to provide a baseline for measuring the absorption spectra of Pc. Extinction coefficients could then be used to determine the relative concentrations of each redox carrier protein in solution. As the oxidised extinction coefficient for Pc is significantly smaller than the reduced extinction coefficients for the cytochromes in this work, small amounts of baseline drift could have a disproportionate impact on concentration estimates for Pc strains. To account for this, rather than using the raw value the OD_{597} for each Pc periplasmic extraction was calculated using the formula (OD_{603} – OD_{700}) x 1.35, where 1.35 is equal to OD_{597}/OD_{700} of pure Pc. Assuming the proportion of total molecules localised in the periplasm remains the same for each redox carrier protein with equal uptake into chromatophores, this technique provides a cheap and high throughput tool for assessing the relative production levels for periplasmic cytochromes and blue copper proteins.

Pyridine Hemochromagen assays

To determine the concentration of iso c_2, for which no published extinction coefficients were available, pyridine hemochromagen assays were carried out using the protocol of Barr and Guo [82], using a reduced extinction coefficient of 30.27 $mM^{-1}cm^{-1}$ for the pyr_2-haem *c* coordination complex [83]. Absorbance spectra were collected on a Cary 60 spectrophotometer with a 1 cm pathlength, and extinction coefficients calculated for 551 nm, the closest whole number to the reduced peak of the heme *c* cofactor in iso c_2. This method gave values as follows: $\varepsilon_{551\ (red)}$ = 25.6 mM^{-1} cm^{-1}, $\varepsilon_{551\ (ox)}$ = 6.53 mM^{-1} cm^{-1} and therefore $\varepsilon_{551\ (red\ -\ ox)}$ = 19.1 mM^{-1} cm^{-1}.

RC-only and RC-LH1 turnover assays

Turnover assays were conducted under steady state conditions in a similar fashion to those described in Martin et al. [53], using 3 x 300 µl solutions containing RC or RC-LH1, soluble redox carrier protein and quinone, in a

solution containing 0.03% (w/v) β-DDM and, where necessary, 1 mM sodium D-ascorbate to keep cytochromes reduced. Each pre-reduced soluble redox carrier protein was added to a concentration at least 20-fold higher than the RC/RC-LH1 complex in solution. Quinones were added in excess from ethanol stock solutions to a final assay concentration of 50 μM, using a volume of < 2 μl to minimise the amount of ethanol in solution.

Following overnight dark adaptation, each 300 μl reaction mixture was placed in a 3 ml, 1 cm pathlength quartz cuvette and monitored at a fixed wavelength using a Cary 60 spectrophotometer (Agilent Technologies). The temperature of the solution was maintained at 25 °C by a Cary Single Cell Peltier Accessory (Agilent Technologies). 10 s into data recording, excitation energy was delivered via a fibre optic cable from an 810 nm M810F2 LED (light-emitting diode) (Thorlabs Ltd., U.K.), typically driven at 100% intensity using a DC2200 controller (Thorlabs Ltd., U.K.) for 20-50 s. Depending on how rapidly the signal changed, the data were processed by fitting the linear initial rate over 0.025–5 s, starting from the first data point where the absorbance started dropping continuously. Rates were normalised to e^-/RC/s by dividing the initial rate by the reduced minus oxidised extinction coefficient for the redox carrier protein, then by the RC or RC-LH1 concentration. All cytochrome extinction coefficients are from either *Rba. sphaeroides* or *Synechocystis* sp. PCC 6803, whilst in the absence of a published extinction coefficient for Pc from *Synechocystis* sp. PCC 6803, the ε_{597} from *Phaseolus vulgaris* (common bean) was used instead [87].

Table 3. Extinction coefficients used in this study

Species	Wavelength	Extinction Coefficient, ε (mM^{-1})	Source
RC-LH1	875	3000	[84]
RC	802	288	[85]
Cyt c_2	550	30.8 (reduced) 21.5 (reduced – oxidised)	[20]

Iso c_2	551	25.6 (reduced) 19.1 (reduced – oxidised)	This study
Cyt c_6	552	24.1 (reduced) 19.5 (reduced-oxidised)	[43] [86]
Pc	597	4.5 (reduced) 4.5 (reduced-oxidised)	[87]
Cyt c	550	27.6 (reduced) 21.1 (reduced – oxidised)	[88]
DUQ	278	14 (oxidised in EtOH	[89]
UQ-2	275	13.7 (oxidised in EtOH)	[89]

Competing Interests

The authors declare that there are no competing interests associated with the manuscript.

Funding

A.G.M.B. was supported by a University of Sheffield Faculty of Science PhD studentship awarded to C.N.H. C.N.H. acknowledges Synergy Award 854126 from the European Research Council, which partially supported E.C.M. and D.J.K.S. A.H. acknowledges a Royal Society University Research Fellowship (award no. URF\R1\191548), which partially supported E.C.M. D.J.K.S. acknowledges start-up funding from the University of East Anglia.

CRediT Author Contribution

Adam G.M. Bowie: Conceptualization, Formal analysis, Investigation, Visualization, Methodology, Writing — original draft, Writing — review and editing.

Andrew Hitchcock: Conceptualization, Formal analysis, Investigation, Supervision, Writing — review and editing.

Matthew S. Proctor: Investigation.

Elizabeth C. Martin: Investigation.

David J.K. Swainsbury: Formal Analysis, Supervision, Investigation, Writing — review and editing.

C. Neil Hunter: Conceptualization, Formal analysis, Resources, Supervision, Funding acquisition, Writing — review and editing.

Abbreviations

BChl, bacteriochlorophyll; cryo-EM, cryogenic electron microscopy; cyt *c*, cytochrome *c* (*Equus caballus*); cyt c_2, cytochrome c_2 (*Rhodobacter sphaeroides*); cyt c_6, cytochrome c_6 (*Synechocystis* sp. PCC 6803); DUQ, decylubiquinone; iso c_2, isocytochrome c_2 (*Rhodobacter sphaeroides*); LED, light-emitting diode; Pc, plastocyanin (*Synechocystis* sp. PCC 6803); PQ, plastoquinone; PSI, photosystem I; PSII, photosystem II; PSIII, photosystem III (proposed); RC-LH1, reaction centre-light harvesting 1; UQ-2, Ubiquinone-2

Data Availability Statement

Any data not provided within the paper as a table, figure or supplementary file is available from the corresponding authors upon request.

References

[1] Blankenship, R. E. (1992) Origin and early evolution of photosynthesis. *Photosynth Res* **33**, 91–111 https://doi.org/10.1007/BF00039173

[2] Sadekar, S., Raymond, J. and Blankenship, R. E. (2006) Conservation of Distantly Related Membrane Proteins: Photosynthetic Reaction Centers Share a Common Structural Core. *Molecular Biology and Evolution* **23**, 2001–2007 https://doi.org/10.1093/molbev/msl079

[3] Orf, G. S., Gisriel, C. and Redding, K. E. (2018) Evolution of photosynthetic reaction centers: insights from the structure of the heliobacterial reaction center. *Photosynth Res* **138**, 11–37 https://doi.org/10.1007/s11120-018-0503-2

[4] Cardona, T., Sánchez-Baracaldo, P., Rutherford, A. W. and Larkum, A. W. (2019) Early Archean origin of Photosystem II. *Geobiology* **17**, 127–150 https://doi.org/10.1111/gbi.12322

[5] Raymond, J. and Blankenship, R. E. (2008) The origin of the oxygen-evolving complex. *Coordination Chemistry Reviews* **252**, 377–383 https://doi.org/10.1016/j.ccr.2007.08.026

[6] Canfield, D. E., Ngombi-Pemba, L., Hammarlund, E. U., Bengtson, S., Chaussidon, M., Gauthier-Lafaye, F., et al. (2013) Oxygen dynamics in the aftermath of the Great Oxidation of Earth's atmosphere. *Proceedings of the National Academy of Sciences*, Proceedings of the National Academy of Sciences **110**, 16736–16741 https://doi.org/10.1073/pnas.1315570110

[7] Blankenship, R. E. (2014) Molecular Mechanisms of Photosynthesis 2nd ed, John Wiley & Sons Incorporated, Hoboken

[8] Johnson, M. P. (2016) Photosynthesis. *Essays in Biochemistry* **60**, 255–273 https://doi.org/10.1042/EBC20160016

[9] Blankenship, R. E., Tiede, D. M., Barber, J., Brudvig, G. W., Fleming, G., Ghirardi, M., et al. (2011) Comparing Photosynthetic and Photovoltaic Efficiencies and Recognizing the Potential for Improvement. *Science*, American Association for the Advancement of Science **332**, 805–809 https://doi.org/10.1126/science.1200165

993 [10] Ort, D. R., Merchant, S. S., Alric, J., Barkan, A., Blankenship, R. E., Bock,
994 R., et al. (2015) Redesigning photosynthesis to sustainably meet global food and
995 bioenergy demand. *Proc. Natl. Acad. Sci. U.S.A.* **112**, 8529–8536
996 https://doi.org/10.1073/pnas.1424031112

997 [11] Hitchcock, A., Hunter, C. N., Sobotka, R., Komenda, J., Dann, M. and
998 Leister, D. (2022) Redesigning the photosynthetic light reactions to enhance
999 photosynthesis – the PhotoRedesign consortium. *The Plant Journal* **109**, 23–
1000 34 https://doi.org/10.1111/tpj.15552

1001 [12] Leister, D. (2023) Enhancing the light reactions of photosynthesis:
1002 Strategies, controversies, and perspectives. *Molecular Plant*, Elsevier **16**, 4–22
1003 https://doi.org/10.1016/j.molp.2022.08.005

1004 [13] Hitchcock, A., Hunter, C. N. and Canniffe, D. P. (2020) Progress and
1005 challenges in engineering cyanobacteria as chassis for light-driven biotechnology.
1006 *Microbial Biotechnology* **13**, 363–367 https://doi.org/10.1111/1751-
1007 7915.13526

1008 [14] Schierenbeck, L., Ries, D., Rogge, K., Grewe, S., Weisshaar, B. and Kruse, O.
1009 (2015) Fast forward genetics to identify mutations causing a high light tolerant
1010 phenotype in *Chlamydomonas reinhardtii* by whole-genome-sequencing. *BMC*
1011 *Genomics* **16**, 57 https://doi.org/10.1186/s12864-015-1232-y

1012 [15] Dann, M., Ortiz, E. M., Thomas, M., Guljamow, A., Lehmann, M., Schaefer,
1013 H., et al. (2021) Enhancing photosynthesis at high light levels by adaptive
1014 laboratory evolution. *Nat. Plants, Nature Publishing Group*, **7**, 681–695
1015 https://doi.org/10.1038/s41477-021-00904-2

1016 [16] Zhao, Z., Vercellino, I., Knoppová, J., Sobotka, R., Murray, J. W., Nixon, P.
1017 J., ... & Komenda, J. (2023). The Ycf48 accessory factor occupies the site of the
1018 oxygen-evolving manganese cluster during photosystem II biogenesis. *Nature*
1019 *communications*, **14**, 4681 https://doi.org/10.1038/s41467-023-40388-6

1020 [17] Gisriel, C. J., Wang, J., Liu, J., Flesher, D. A., Reiss, K. M., Huang, H. L., ...
1021 & Brudvig, G. W. (2022). High-resolution cryo-electron microscopy structure of

photosystem II from the mesophilic cyanobacterium, *Synechocystis* sp. PCC 6803. *Proceedings of the National Academy of Sciences*, **119**, e2116765118 https://doi.org/10.1073/pnas.2116765118

[18] Proctor, M. S., Malone, L. A., Farmer, D. A., Swainsbury, D. J., Hawkings, F. R., Pastorelli, F., ... & Hitchcock, A. (2022). Cryo-EM structures of the *Synechocystis* sp. PCC 6803 cytochrome b_6f complex with and without the regulatory PetP subunit. *Biochemical Journal*, **479**, 1487-1503. https://doi.org/10.1042/BCJ20220124

[19] Qian, P., Swainsbury, D. J. K., Croll, T. I., Salisbury, J. H., Martin, E. C., Jackson, P. J., et al. (2021) Cryo-EM structure of the monomeric *Rhodobacter sphaeroides* RC–LH1 core complex at 2.5 Å. *Biochemical Journal* **478**, 3775–3790 https://doi.org/10.1042/BCJ20210631

[20] Axelrod, H. L., Abresch, E. C., Okamura, M. Y., Yeh, A. P., Rees, D. C. and Feher, G. (2002) X-ray Structure Determination of the Cytochrome c_2: Reaction Center Electron Transfer Complex from *Rhodobacter sphaeroides*. *Journal of Molecular Biology* **319**, 501–515 https://doi.org/10.1016/S0022-2836(02)00168-7

[21] Busch, A. and Hippler, M. (2011) The structure and function of eukaryotic photosystem I. *Biochimica et Biophysica Acta (BBA) - Bioenergetics* **1807**, 864–877 https://doi.org/10.1016/j.bbabio.2010.09.009

[22] Wachtveitl, J., Farchaus, J. W., Mathis, P. and Oesterhelt, D. (1993) Tyrosine 162 of the photosynthetic reaction center L-subunit plays a critical role in the cytochrome c_2 mediated rereduction of the photooxidized bacteriochlorophyll dimer in *Rhodobacter sphaeroides*. Quantitative kinetic analysis. *Biochemistry* **32**, 10894–10904 https://doi.org/10.1021/bi00091a045

[23] Farchaus, J. W., Wachtveitl, J., Mathis, P. and Oesterhelt, D. (1993) Tyrosine 162 of the photosynthetic reaction center L-subunit plays a critical role in the cytochrome c_2 mediated rereduction of the photooxidized

bacteriochlorophyll dimer in *Rhodobacter sphaeroides*. 1. Site-directed mutagenesis and initial characterization. *Biochemistry* **32**, 10885–10893 https://doi.org/10.1021/bi00091a044

[24] Jordan, P., Fromme, P., Witt, H. T., Klukas, O., Saenger, W. and Krauß, N. (2001) Three-dimensional structure of cyanobacterial photosystem I at 2.5 Å resolution. *Nature*, Nature Publishing Group **411**, 909–917 https://doi.org/10.1038/35082000

[25] Sommer, F., Drepper, F. and Hippler, M. (2002) The Luminal Helix I of PsaB Is Essential for Recognition of Plastocyanin or Cytochrome c_6 and Fast Electron Transfer to Photosystem I in *Chlamydomonas reinhardtii*. *Journal of Biological Chemistry*, Elsevier **277**, 6573–6581 https://doi.org/10.1074/jbc.M110633200

[26] Sommer, F., Drepper, F., Haehnel, W. and Hippler, M. (2004) The Hydrophobic Recognition Site Formed by Residues PsaA-Trp651 and PsaB-Trp627 of Photosystem I in *Chlamydomonas reinhardtii* Confers Distinct Selectivity for Binding of Plastocyanin and Cytochrome c_6. *Journal of Biological Chemistry*, Elsevier **279**, 20009–20017 https://doi.org/10.1074/jbc.M313986200

[27] Axelrod, H. L. and Okamura, M. Y. (2005) The structure and function of the cytochrome c_2: reaction center electron transfer complex from *Rhodobacter sphaeroides*. *Photosynth Res* **85**, 101–114 https://doi.org/10.1007/s11120-005-1368-8

[28] Vasilev, C., Nguyen, J., Bowie, A. G. M., Mayneord, G. E., Martin, E. C., Hitchcock, A., et al. (2024) Single-Molecule Detection of the Encounter and Productive Electron Transfer Complexes of a Photosynthetic Reaction Center. *J. Am. Chem. Soc.*, American Chemical Society **146**, 20019–20032 https://doi.org/10.1021/jacs.4c03913

[29] Caspy, I., Fadeeva, M., Kuhlgert, S., Borovikova-Sheinker, A., Klaiman, D., Masrati, G., et al. (2021) Structure of plant photosystem I-plastocyanin

complex reveals strong hydrophobic interactions. *Biochemical Journal* **478**, 2371–2384 https://doi.org/10.1042/BCJ20210267

[30] Redinbo, M. R., Yeates, T. O. and Merchant, S. (1994) Plastocyanin: Structural and functional analysis. *J Bioenerg Biomembr* **26**, 49–66 https://doi.org/10.1007/BF00763219

[31] Ramesh, V. M., Guergova-Kuras, M., Joliot, P. and Webber, A. N. (2002) Electron Transfer from Plastocyanin to the Photosystem I Reaction Center in Mutants with Increased Potential of the Primary Donor in *Chlamydomonas reinhardtii*. *Biochemistry*, American Chemical Society **41**, 14652–14658 https://doi.org/10.1021/bi026392z

[32] Díaz-Quintana, A., Navarro, J. A., Hervás, M., Molina-Heredia, F. P., De la Cerda, B. and De la Rosa, M. A. (2003) A comparative structural and functional analysis of cyanobacterial plastocyanin and cytochrome c_6 as alternative electron donors to Photosystem I. *Photosynthesis Research* **75**, 97–110 https://doi.org/10.1023/A:1022841513592

[33] Frazão, C., Soares, C. M., Carrondo, M. A., Pohl, E., Dauter, Z., Wilson, K. S., et al. (1995) *Ab initio* determination of the crystal structure of cytochrome c_6 and comparison with plastocyanin. *Structure*, Elsevier **3**, 1159–1169 https://doi.org/10.1016/S0969-2126(01)00252-0

[34] De la Cerda, B., Castielli, O., Durán, R. V., Navarro, J. A., Hervás, M. and De la Rosa, M. A. (2007) A proteomic approach to iron and copper homeostasis in cyanobacteria. *Briefings in Functional Genomics* **6**, 322–329 https://doi.org/10.1093/bfgp/elm030

[35] Aitken, A. (1975) Prokaryote-eukaryote relationship and the amino acid sequence of plastocyanin from *Anabaena variabilis*. *Biochemical Journal* **149**, 675–683 https://doi.org/10.1042/bj1490675

[36] Chitnis, P. R., Purvis, D. and Nelson, N. (1991) Molecular cloning and targeted mutagenesis of the gene psaF encoding subunit III of photosystem I

from the cyanobacterium *Synechocystis* sp. PCC 6803. *Journal of Biological Chemistry* **266**, 20146–20151 https://doi.org/10.1016/S0021-9258(18)54902-4

[37] Hope, A. B. (2000) Electron transfers amongst cytochrome *f*, plastocyanin and photosystem I: kinetics and mechanisms. *Biochimica et Biophysica Acta (BBA) - Bioenergetics* **1456**, 5–26 https://doi.org/10.1016/S0005-2728(99)00101-2

[38] Moser, C. C., Keske, J. M., Warncke, K., Farid, R. S. and Dutton, P. L. (1992) Nature of biological electron transfer. *Nature*, Nature Publishing Group **355**, 796–802 https://doi.org/10.1038/355796a0

[39] Page, C. C., Moser, C. C., Chen, X. and Dutton, P. L. (1999) Natural engineering principles of electron tunnelling in biological oxidation–reduction. *Nature*, Nature Publishing Group **402**, 47–52 https://doi.org/10.1038/46972

[40] Moser, C. C., Anderson, J. L. R. and Dutton, P. L. (2010) Guidelines for tunneling in enzymes. *Biochimica et Biophysica Acta (BBA) - Bioenergetics* **1797**, 1573–1586 https://doi.org/10.1016/j.bbabio.2010.04.441

[41] Abramson, J., Adler, J., Dunger, J., Evans, R., Green, T., Pritzel, A., et al. (2024) Accurate structure prediction of biomolecular interactions with AlphaFold 3. *Nature*, Nature Publishing Group **630**, 493–500 https://doi.org/10.1038/s41586-024-07487-w

[42] Rott, M. A. and Donohue, T. J. (1990) *Rhodobacter sphaeroides* spd mutations allow cytochrome c_2-independent photosynthetic growth. *Journal of Bacteriology*, American Society for Microbiology **172**, 1954–1961 https://doi.org/10.1128/jb.172.4.1954-1961.1990

[43] Díaz, A., Navarro, F., Hervás, M., Navarro, J. A., Chávez, S., Florencio, F. J., et al. (1994) Cloning and correct expression in *E. coli* of the *petJ* gene encoding

cytochrome c_6 from *Synechocystis* 6803. *FEBS Letters* **347**, 173–177 https://doi.org/10.1016/0014-5793(94)00529-X

[44] Pettigrew, G. W., Meyer, T. E., Bartsch, R. G. and Kamen, M. D. (1976) pH dependence of the oxidation-reduction potential of cytochrome c_2. *Biochimica et Biophysica Acta (BBA) - Bioenergetics* **430**, 197–208 https://doi.org/10.1016/0005-2728(76)90079-7

[45] Rott, M. A., Fitch, J., Meyer, T. E. and Donohue, T. J. (1992) Regulation of a cytochrome c_2 isoform in wild-type and cytochrome c_2 mutant strains of *Rhodobacter sphaeroides*. *Archives of Biochemistry and Biophysics* **292**, 576–582 https://doi.org/10.1016/0003-9861(92)90033-S

[46] Honorato, R. V., Koukos, P. I., Jiménez-García, B., Tsaregorodtsev, A., Verlato, M., Giachetti, A., et al. (2021) Structural Biology in the Clouds: The WeNMR-EOSC Ecosystem. *Front. Mol. Biosci.*, Frontiers **8** https://doi.org/10.3389/fmolb.2021.729513

[47] Honorato, R. V., Roel-Touris, J. and Bonvin, A. M. J. J. (2019) MARTINI-Based Protein-DNA Coarse-Grained HADDOCKing. *Front. Mol. Biosci.*, Frontiers **6** https://doi.org/10.3389/fmolb.2019.00102

[48] Visschers, R. W., Vulto, S. I. E., Jones, M. R., Grondelle, R. van and Kraayenhof, R. (1999) Functional LH1 antenna complexes influence electron transfer in bacterial photosynthetic reaction centers. *Photosynthesis Research* **59**, 95–104 https://doi.org/10.1023/A:1006169201579

[49] Nakamura, A., Suzawa, T., Kato, Y. and Watanabe, T. (2011) Species Dependence of the Redox Potential of the Primary Electron Donor P700 in Photosystem I of Oxygenic Photosynthetic Organisms Revealed by Spectroelectrochemistry. *Plant and Cell Physiology* **52**, 815–823 https://doi.org/10.1093/pcp/pcr034

[50] Lin, X., Williams, J. C., Allen, J. P. and Mathis, P. (1994) Relationship between rate and free energy difference for electron transfer from cytochrome

c_2 to the reaction center in *Rhodobacter sphaeroides*. *Biochemistry*, American Chemical Society **33**, 13517–13523 https://doi.org/10.1021/bi00250a002

[51] Jumper, J., Evans, R., Pritzel, A., Green, T., Figurnov, M., Ronneberger, O., et al. (2021) Highly accurate protein structure prediction with AlphaFold. *Nature*, Nature Publishing Group **596**, 583–589 https://doi.org/10.1038/s41586-021-03819-2

[52] Jurrus, E., Engel, D., Star, K., Monson, K., Brandi, J., Felberg, L. E., et al. (2018) Improvements to the APBS biomolecular solvation software suite. *Protein Science* **27**, 112–128 https://doi.org/10.1002/pro.3280

[53] Martin, E. C., Bowie, A. G. M., Wellfare Reid, T., Neil Hunter, C., Hitchcock, A. and Swainsbury, D. J. K. (2024) Sulfoquinovosyl diacylglycerol is required for dimerisation of the *Rhodobacter sphaeroides* reaction centre–light harvesting 1 core complex. *Biochemical Journal* **481**, 823–838 https://doi.org/10.1042/BCJ20240125

[54] Tikh, I. B., Held, M. and Schmidt-Dannert, C. (2014) BioBrick™ compatible vector system for protein expression in *Rhodobacter sphaeroides*. *Appl Microbiol Biotechnol* **98**, 3111–3119 https://doi.org/10.1007/s00253-014-5527-8

[55] Witthuhn, Vernon C., Gao, J., Hong, S., Halls, S., Rott, M. A., Wraight, C. A., et al. (1997) Reactions of Isocytochrome c_2 in the Photosynthetic Electron Transfer Chain of *Rhodobacter sphaeroides*. *Biochemistry*, American Chemical Society **36**, 903–911 https://doi.org/10.1021/bi961648k

[56] Rott, M. A. and Donohue, T. J. (1990) *Rhodobacter sphaeroides* spd mutations allow cytochrome c_2-independent photosynthetic growth. *Journal of Bacteriology*, American Society for Microbiology **172**, 1954–1961 https://doi.org/10.1128/jb.172.4.1954-1961.1990

[57] Lilburn, T. G., Haith, C. E., Prince, R. C. and Beatty, J. T. (1992) Pleiotropic effects of *pufX* gene deletion on the structure and function of the

photosynthetic apparatus of *Rhodobacter capsulatus*. *Biochimica et Biophysica Acta (BBA) - Bioenergetics* **1100**, 160–170 https://doi.org/10.1016/0005-2728(92)90077-F

[58] Chidgey, J. W., Jackson, P. J., Dickman, M. J. and Hunter, C. N. (2017) PufQ regulates porphyrin flux at the haem/bacteriochlorophyll branchpoint of tetrapyrrole biosynthesis via interactions with ferrochelatase. *Molecular Microbiology* **106**, 961–975 https://doi.org/10.1111/mmi.13861

[59] Overfield, R. E., Wraight, C. A. and Devault, D. (1979) Microsecond photooxidation kinetics of cytochrome c_2 from *Rhodopseudomonas sphaeroides*: in vivo and solution studies. *FEBS letters* **105**, 137–142 https://doi.org/10.1016/0014-5793(79)80903-5

[60] Gerencsér, L., Laczkó, G. and Maróti, P. (1999) Unbinding of Oxidized Cytochrome *c* from Photosynthetic Reaction Center of Rhodobacter sphaeroides Is the Bottleneck of Fast Turnover. *Biochemistry*, American Chemical Society **38**, 16866–16875 https://doi.org/10.1021/bi991563u

[61] Reed, D. W. and Clayton, R. K. (1968) Isolation of a reaction center fraction from *Rhodopseudomonas spheroides*. *Biochemical and Biophysical Research Communications* **30**, 471–475 https://doi.org/10.1016/0006-291X(68)90075-2

[62] Peschek, G. A. (1999) Photosynthesis and Respiration of Cyanobacteria. In The Phototrophic Prokaryotes (Peschek, G. A., Löffelhardt, W., and Schmetterer, G., eds.), pp 201–209, Springer US, Boston, MA https://doi.org/10.1007/978-1-4615-4827-0_24

[63] Hervás, M., Navarro, J. A. and De la Rosa, M. A. (2003) Electron Transfer between Membrane Complexes and Soluble Proteins in Photosynthesis. *Acc. Chem. Res.*, American Chemical Society **36**, 798–805 https://doi.org/10.1021/ar020084b

[64] Drepper, F., Hippler, M., Nitschke, W. and Haehnel, W. (1996) Binding Dynamics and Electron Transfer between Plastocyanin and Photosystem I. *Biochemistry*, American Chemical Society **35**, 1282–1295 https://doi.org/10.1021/bi951471e

[65] Tetreault, M., Rongey, S. H., Feher, G. and Okamura, M. Y. (2001) Interaction between Cytochrome c_2 and the Photosynthetic Reaction Center from *Rhodobacter sphaeroides*: Effects of Charge-Modifying Mutations on Binding and Electron Transfer. *Biochemistry*, American Chemical Society **40**, 8452–8462 https://doi.org/10.1021/bi010222p

[66] Swainsbury, D. J. K., Qian, P., Jackson, P. J., Faries, K. M., Niedzwiedzki, D. M., Martin, E. C., et al. (2021) Structures of *Rhodopseudomonas palustris* RC-LH1 complexes with open or closed quinone channels. *Science Advances*, American Association for the Advancement of Science **7**, eabe2631 https://doi.org/10.1126/sciadv.abe2631

[67] Mao, R., Guo, J., Bie, L., Liu, L.-N. and Gao, J. (2024) Tunneling Mechanisms of Quinones in Photosynthetic Reaction Center–Light Harvesting 1 Supercomplexes. *Small Science* **4**, 2400188 https://doi.org/10.1002/smsc.202400188

[68] Swainsbury, D. J. K., Qian, P., Hitchcock, A. and Hunter, C. N. (2023) The structure and assembly of reaction centre-light-harvesting 1 complexes in photosynthetic bacteria. *Bioscience Reports* **43**, BSR20220089 https://doi.org/10.1042/BSR20220089

[69] Qian, P., Papiz, M. Z., Jackson, P. J., Brindley, A. A., Ng, I. W., Olsen, J. D., et al. (2013) Three-Dimensional Structure of the *Rhodobacter sphaeroides* RC-LH1-PufX Complex: Dimerization and Quinone Channels Promoted by PufX. *Biochemistry*, American Chemical Society **52**, 7575–7585 https://doi.org/10.1021/bi4011946

[70] Semchonok, D. A., Siponen, M. I., Tüting, C., Charras, Q., Kyrilis, F. L., Hamdi, F., et al. (2022, March 1) Cryo-EM structure of the *Rhodobaca*

bogoriensis RC-LH1-PufX dimeric complex at 2.9 Å, bioRxiv https://doi.org/10.1101/2022.02.25.481955

[71] Tani, K., Kanno, R., Kikuchi, R., Kawamura, S., Nagashima, K. V. P., Hall, M., et al. (2022) Asymmetric structure of the native *Rhodobacter sphaeroides* dimeric LH1–RC complex. *Nat Commun*, Nature Publishing Group **13**, 1904 https://doi.org/10.1038/s41467-022-29453-8

[72] Cao, P., Bracun, L., Yamagata, A., Christianson, B. M., Negami, T., Zou, B., et al. (2022) Structural basis for the assembly and quinone transport mechanisms of the dimeric photosynthetic RC–LH1 supercomplex. *Nat Commun*, Nature Publishing Group **13**, 1977 https://doi.org/10.1038/s41467-022-29563-3

[73] Geyer, T. and Helms, V. (2006) Reconstruction of a Kinetic Model of the Chromatophore Vesicles from *Rhodobacter sphaeroides*. *Biophysical Journal* **91**, 927–937 https://doi.org/10.1529/biophysj.105.067561

[74] Cartron, M. L., Olsen, J. D., Sener, M., Jackson, P. J., Brindley, A. A., Qian, P., et al. (2014) Integration of energy and electron transfer processes in the photosynthetic membrane of *Rhodobacter sphaeroides*. *Biochimica et Biophysica Acta (BBA) - Bioenergetics* **1837**, 1769–1780 https://doi.org/10.1016/j.bbabio.2014.02.003

[75] Sener, M., Strumpfer, J., Singharoy, A., Hunter, C. N. and Schulten, K. (2016) Overall energy conversion efficiency of a photosynthetic vesicle. *eLife* (Hummer, G., ed.), eLife Sciences Publications, Ltd **5**, e09541 https://doi.org/10.7554/eLife.09541

[76] Vasilev, C., Mayneord, G.E., Brindley, A.A., Johnson, M.P. and Hunter, C.N. (2019) Dissecting the cytochrome c_2–reaction centre interaction in bacterial photosynthesis using single molecule force spectroscopy. *Biochemical Journal* **476**, 2173–2190. https://doi.org/10.1042/BCJ20170519.

[77] Sutherland, G. A., Qian, P., Hunter, C. N., Swainsbury, D. J. K. and Hitchcock, A. (2022) Chapter Five - Engineering purple bacterial carotenoid biosynthesis to study the roles of carotenoids in light-harvesting complexes. In Methods in Enzymology (Wurtzel, E. T., ed.), pp 137–184, Academic Press https://doi.org/10.1016/bs.mie.2022.04.001

[78] Swainsbury, D. J. K., Martin, E. C., Vasilev, C., Parkes-Loach, P. S., Loach, P. A. and Neil Hunter, C. (2017) Engineering of a calcium-ion binding site into the RC-LH1-PufX complex of *Rhodobacter sphaeroides* to enable ion-dependent spectral red-shifting. *Biochimica et Biophysica Acta (BBA) - Bioenergetics* **1858**, 927–938 https://doi.org/10.1016/j.bbabio.2017.08.009

[79] Qian, P., Martin, E. C., Ng, I. W. and Hunter, C. N. (2017) The C-terminus of PufX plays a key role in dimerisation and assembly of the reaction center light-harvesting 1 complex from *Rhodobacter sphaeroides*. *Biochim Biophys Acta* **1858**, 795–803 https://doi.org/10.1016/j.bbabio.2017.06.001

[80] Simon, R., Priefer, U. and Pühler, A. (1983) A Broad Host Range Mobilization System for *In Vivo* Genetic Engineering: Transposon Mutagenesis in Gram Negative Bacteria. *Nat Biotechnol*, Nature Publishing Group **1**, 784–791 https://doi.org/10.1038/nbt1183-784

[81] Hunter, C. N. and Turner, G. (1988) Transfer of Genes Coding for Apoproteins of Reaction Centre and Light-harvesting LH1 Complexes to *Rhodobacter sphaeroides*. *Microbiology*, Microbiology Society, **134**, 1471–1480 https://doi.org/10.1099/00221287-134-6-1471

[82] Barr, I. and Guo, F. (2015) Pyridine Hemochromagen Assay for Determining the Concentration of Heme in Purified Protein Solutions. *Bio Protoc* **5**, e1594 https://doi.org/10.21769/bioprotoc.1594

[83] Berry, E. A. and Trumpower, B. L. (1987) Simultaneous determination of hemes *a*, *b*, and *c* from pyridine hemochrome spectra. *Analytical Biochemistry* **161**, 1–15 https://doi.org/10.1016/0003-2697(87)90643-9

[84] Huang, X., Vasilev, C., Swainsbury, D. J. K. and Hunter, C. N. (2024) Excitation energy transfer in proteoliposomes reconstituted with LH2 and RC-LH1 complexes from *Rhodobacter sphaeroides*. *Bioscience Reports* **44**, BSR20231302 https://doi.org/10.1042/BSR20231302

[85] Straley, S. C., Parson, W. W., Mauzerall, D. C. and Clayton, R. K. (1973) Pigment content and molar extinction coefficients of photochemical reaction centers from *Rhodopseudomonas spheroides*. *Biochimica et Biophysica Acta (BBA) - Bioenergetics* **305**, 597–609 https://doi.org/10.1016/0005-2728(73)90079-0

[86] Cho, Y. S., Wang, Q. J., Krogmann, D. and Whitmarsh, J. (1999) Extinction coefficients and midpoint potentials of cytochrome c_6 from the cyanobacteria *Arthrospira maxima*, *Microcystis aeruginosa*, and *Synechocystis* 6803. *Biochimica et Biophysica Acta (BBA) - Bioenergetics* **1413**, 92–97 https://doi.org/10.1016/S0005-2736(99)00124-8

[87] Milne, P. R. and Wells, J. R. E. (1970) Structural and Molecular Weight Studies on the Small Copper Protein, Plastocyanin. *Journal of Biological Chemistry*, Elsevier **245**, 1566–1574 https://doi.org/10.1016/S0021-9258(19)77132-4

[88] Margoliash, E. and Walasek, O. F. (1967) Cytochrome *c* from vertebrate and invertebrate sources. In Methods in Enzymology, pp 339–348, Academic Press https://doi.org/10.1016/0076-6879(67)10064-5

[89] Fato, R., Estornell, E., Di Bernardo, S., Pallotti, F., Parenti Castelli, G. and Lenaz, G. (1996) Steady-State Kinetics of the Reduction of Coenzyme Q Analogs by Complex I (NADH:Ubiquinone Oxidoreductase) in Bovine Heart Mitochondria and Submitochondrial Particles. *Biochemistry*, American Chemical Society **35**, 2705–2716 https://doi.org/10.1021/bi9516034

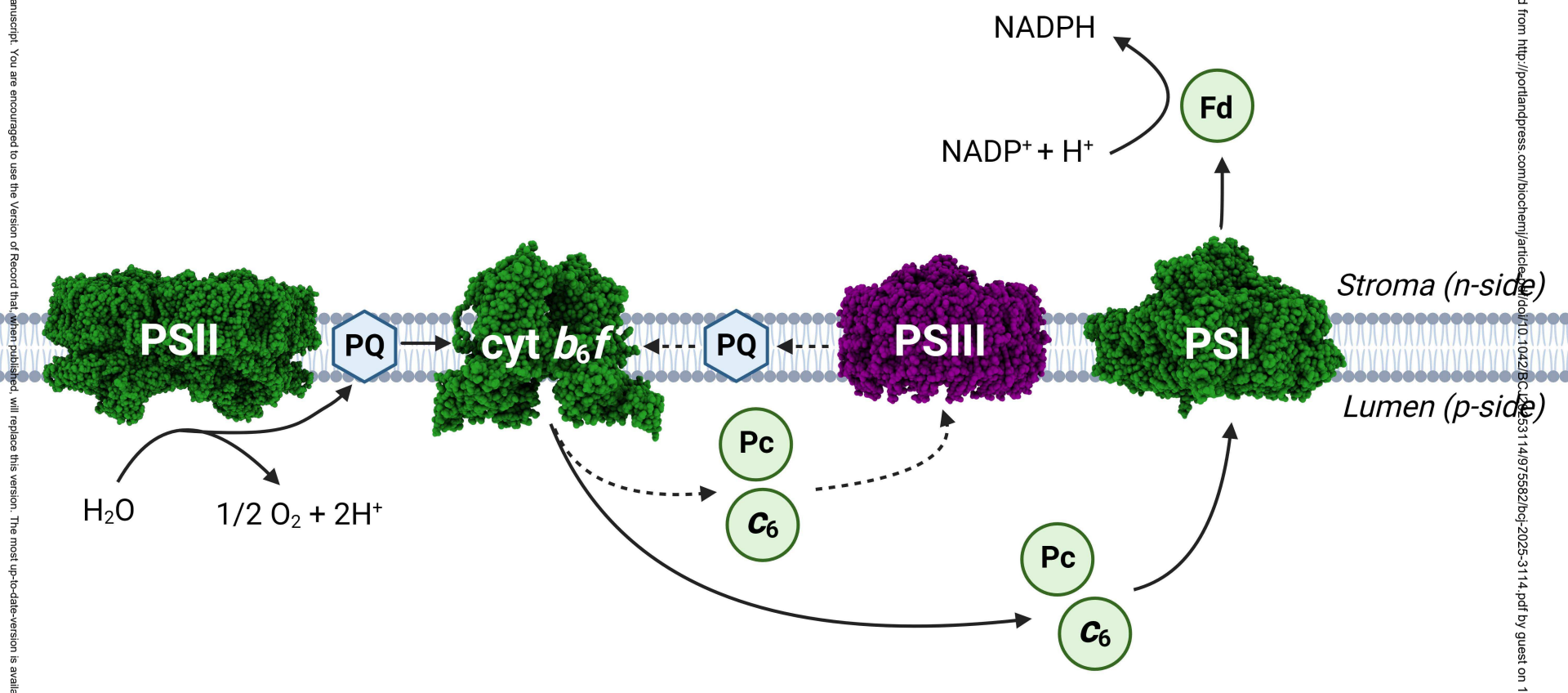

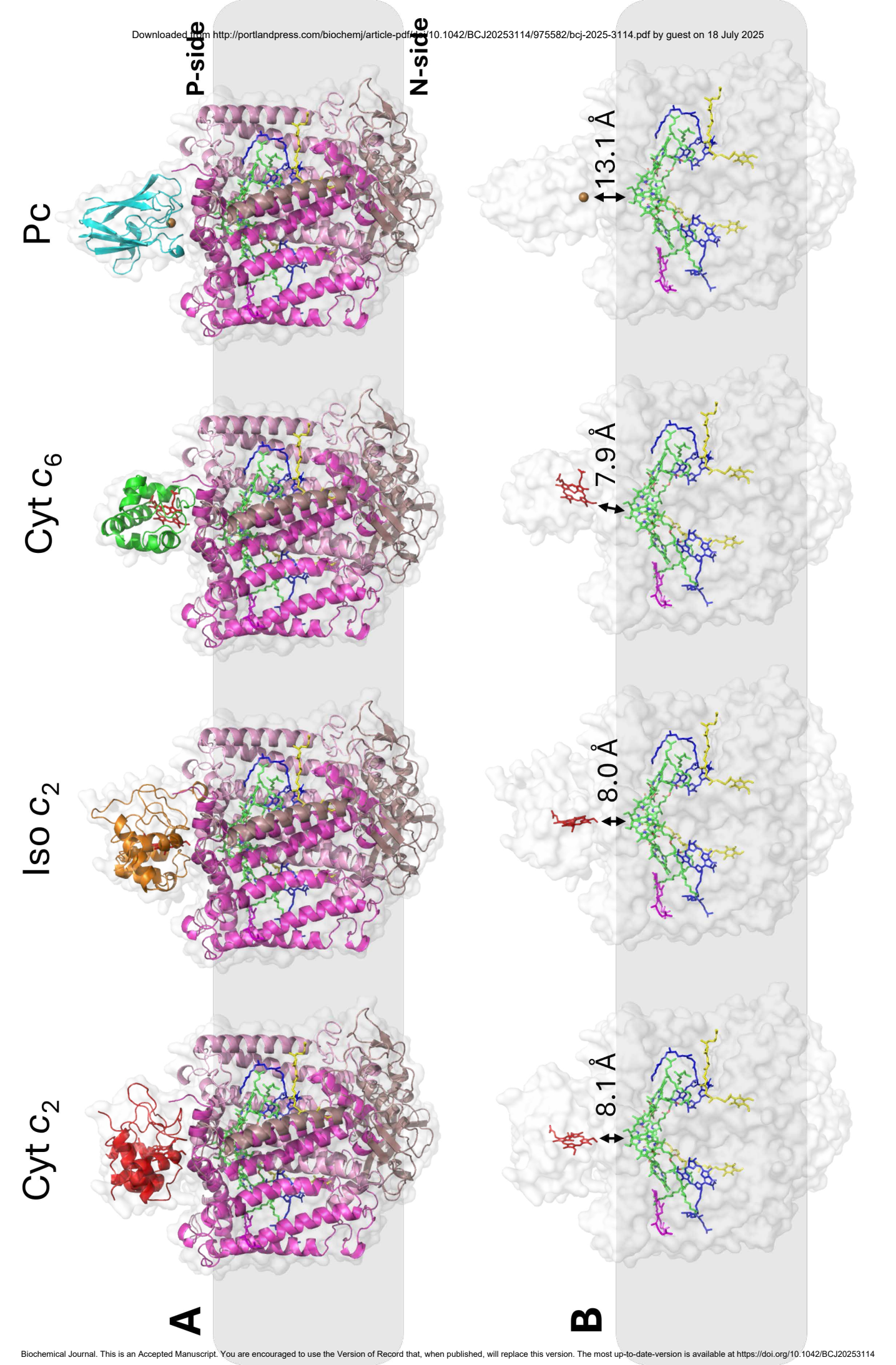

A

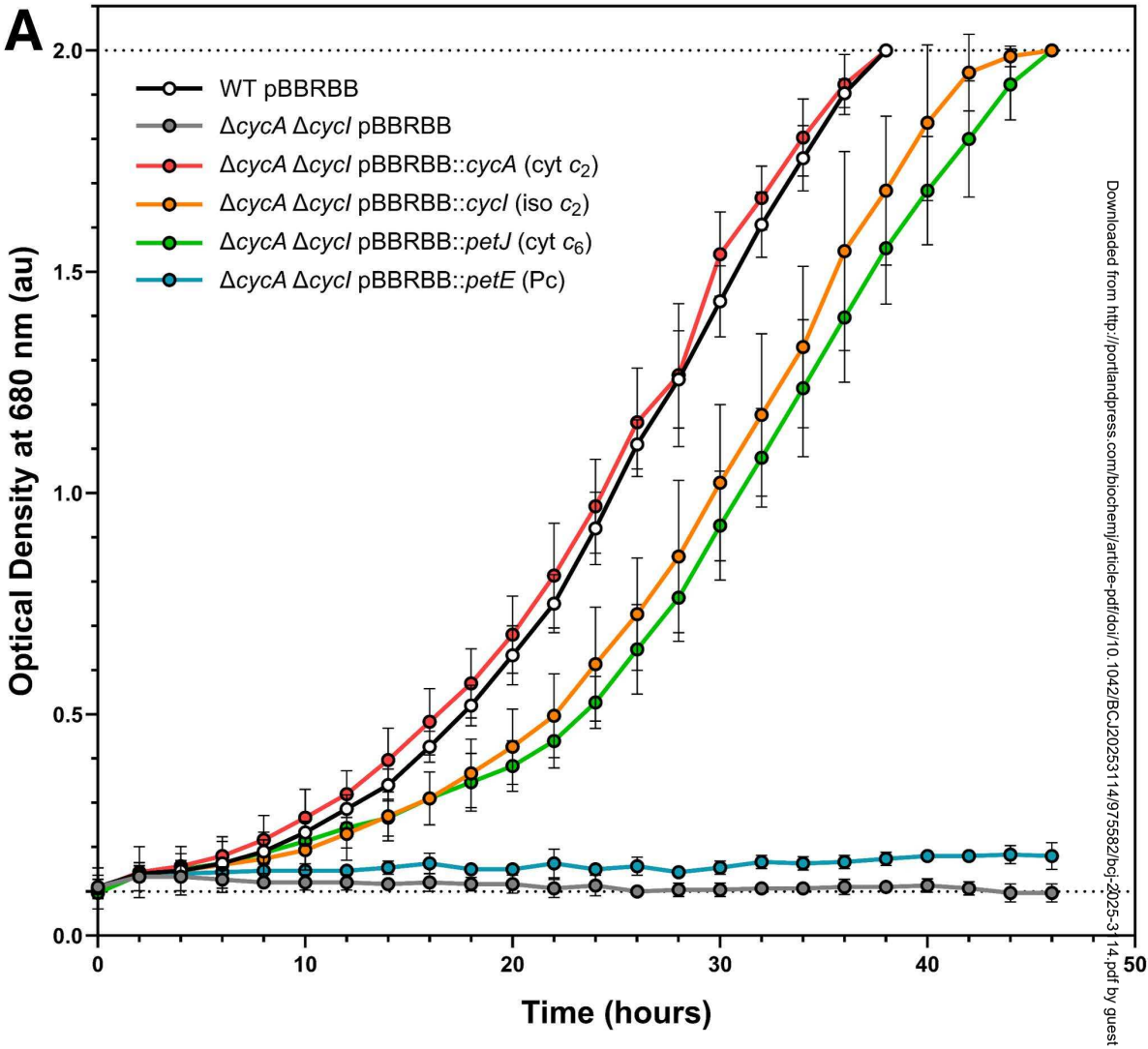

B

Transconjugant Strain	Rate Constant (*k*)	Doubling Time (hours)
WT pBBRBB	0.074	9.42
ΔcycA ΔcycI pBBRBB	-0.005	-
ΔcycA ΔcycI pBBRBB::*cycA*	0.076	9.15
ΔcycA ΔcycI pBBRBB::*cycI*	0.072	9.69
ΔcycA ΔcycI pBBRBB::*petJ*	0.067	10.3
ΔcycA ΔcycI pBBRBB::*petE*	0.007	103

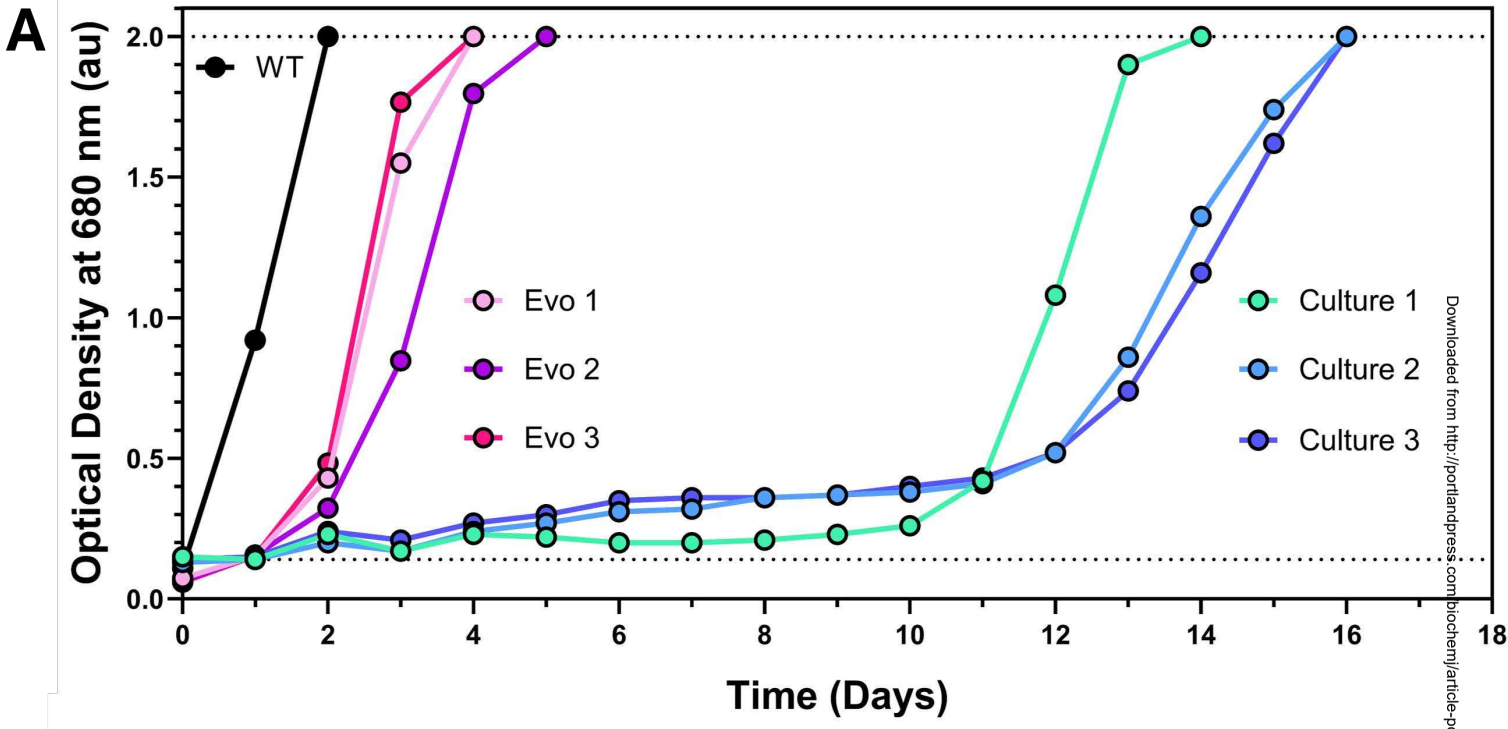

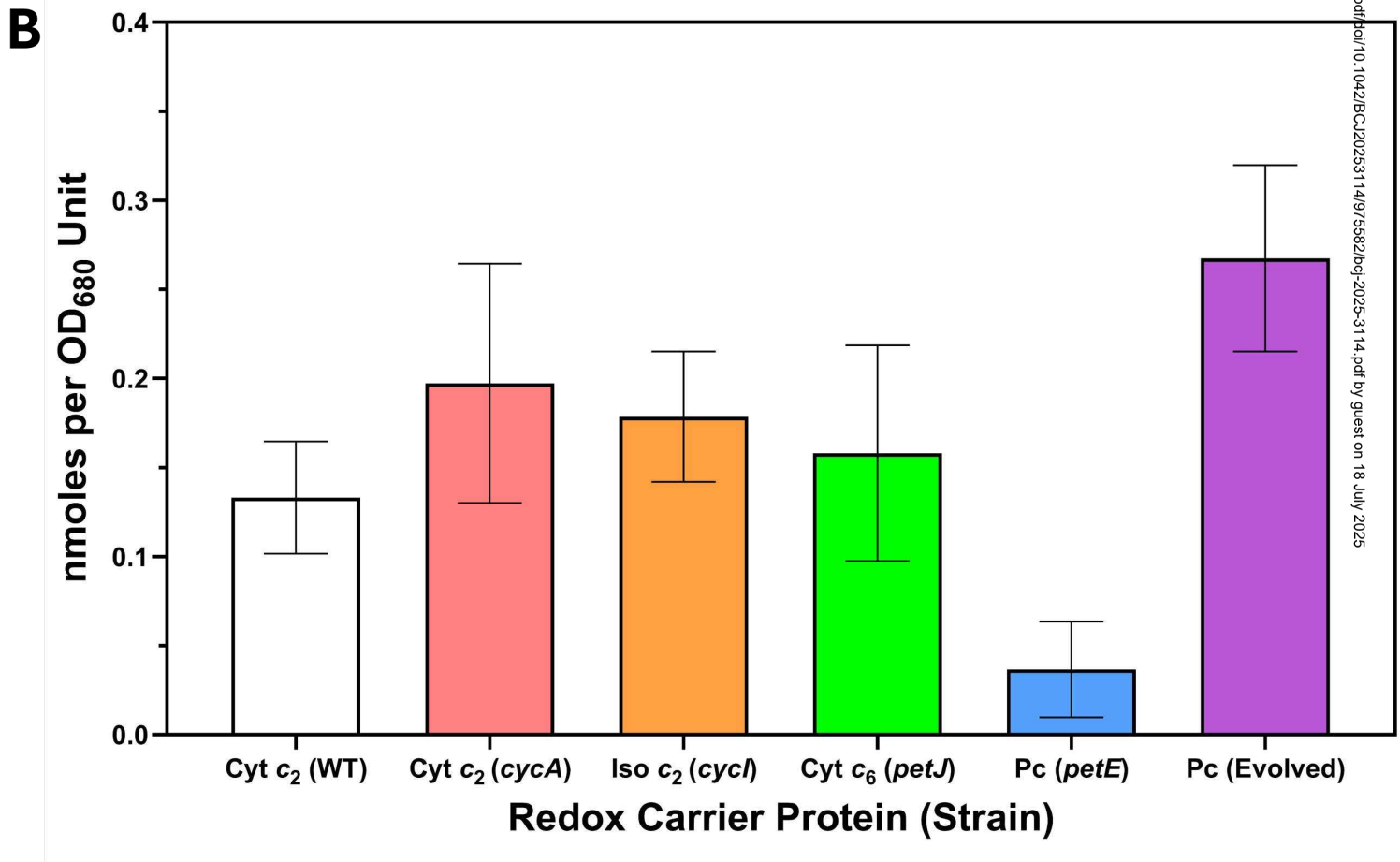

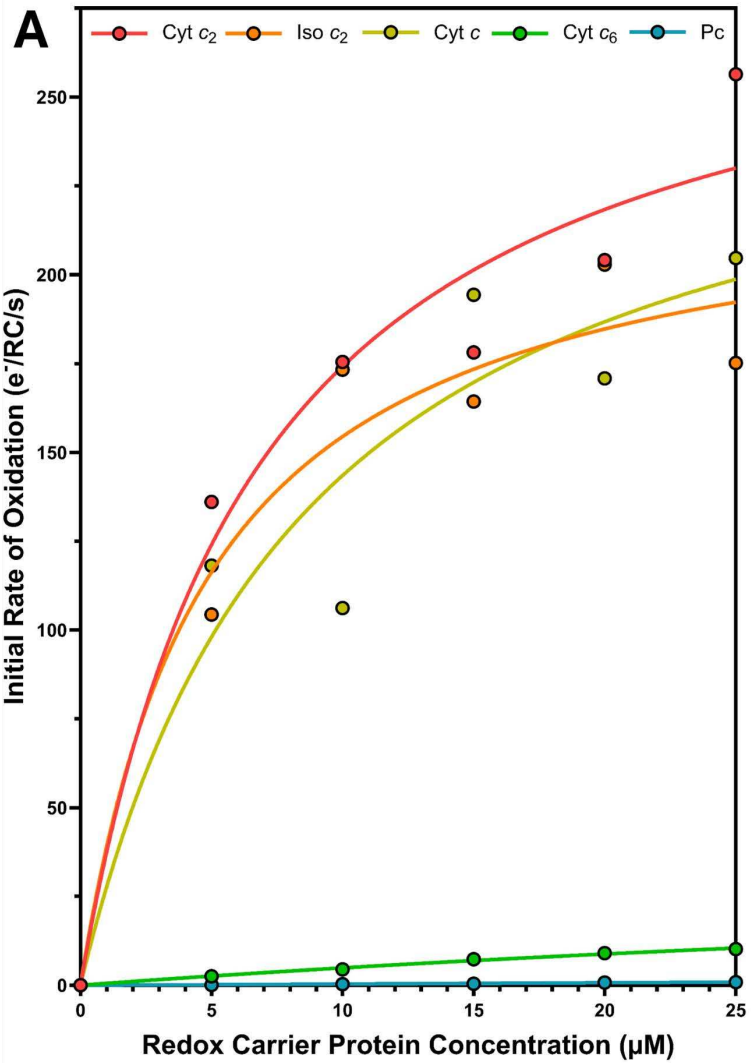

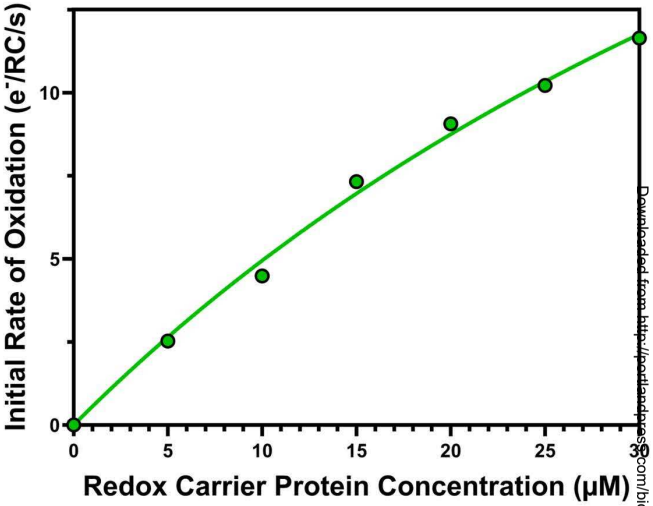

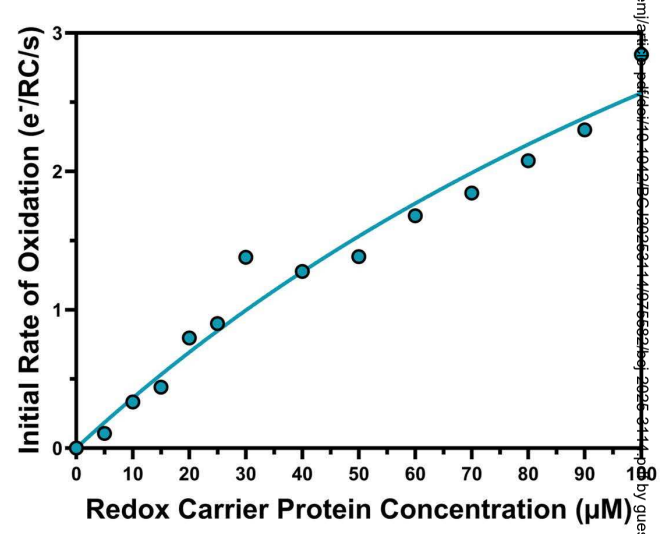

D

Redox Carrier Protein	V_{max} (e^-/RC/s) (Best Estimate)	V_{max} (e^-/RC/s) (95 % CI)	K_M (μM) (Best Estimate)	K_M (μM) (95 % CI)	R Squared
Cyt c_2	293	218 – 473	6.80	1.89 – 21.2	0.833
Iso c_2	230	189 – 293	5.88	1.94 – 10.3	0.890
Cyt c	267	190 – 469	8.63	2.49 – 27.9	0.837
Cyt c_6	37.8	25.5 – 77.1	66.3	37.80– 160	0.975
Pc	7.92	5.42 – 15.8	209	121 – 488	0.951

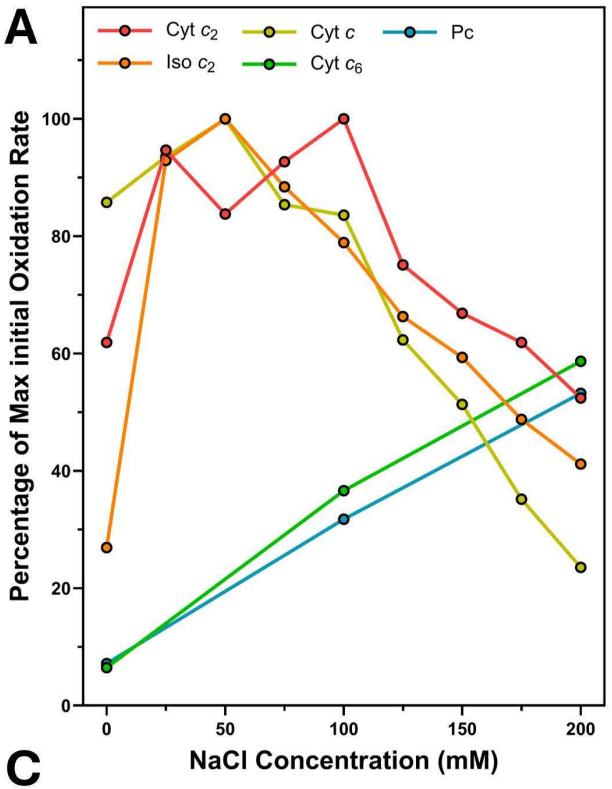

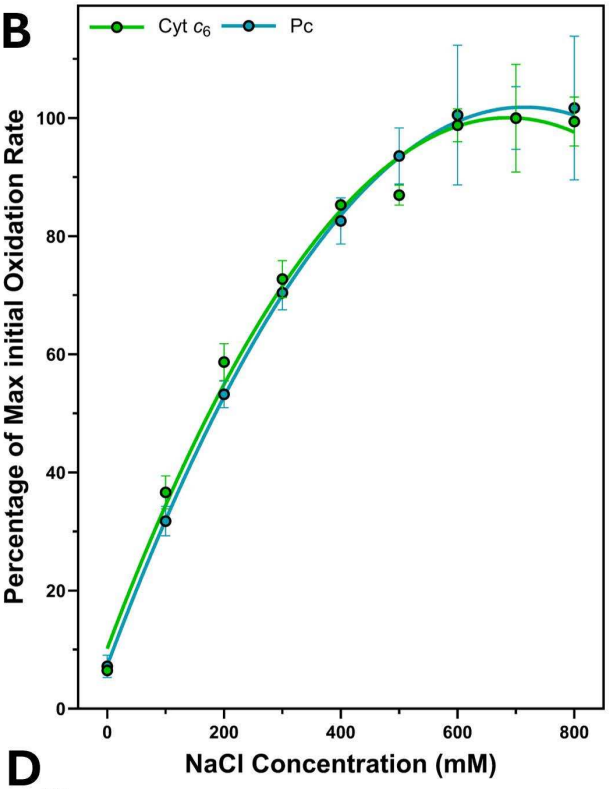

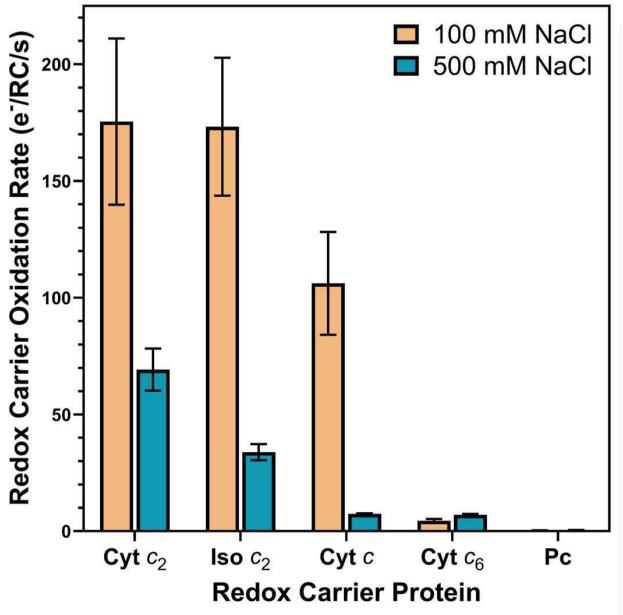

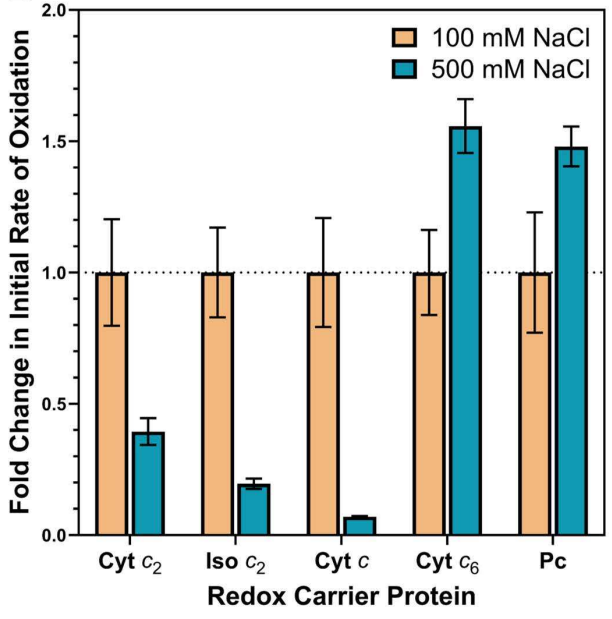

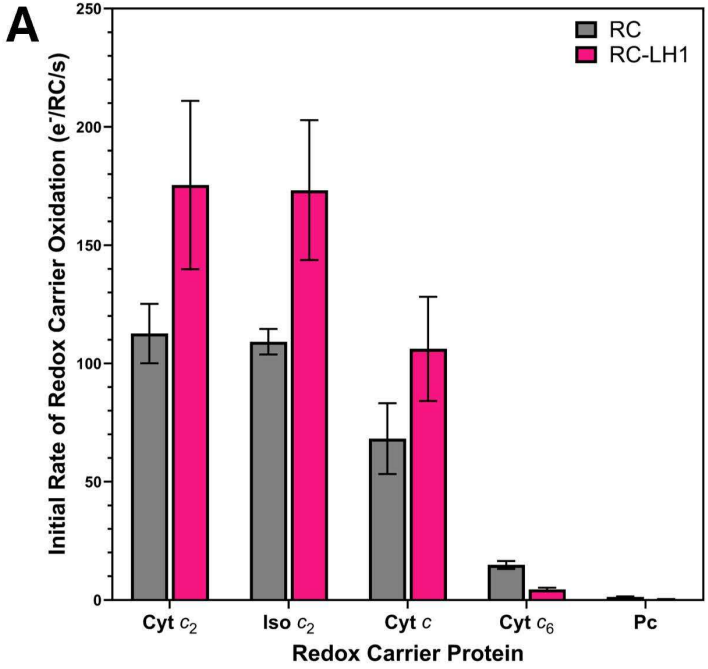

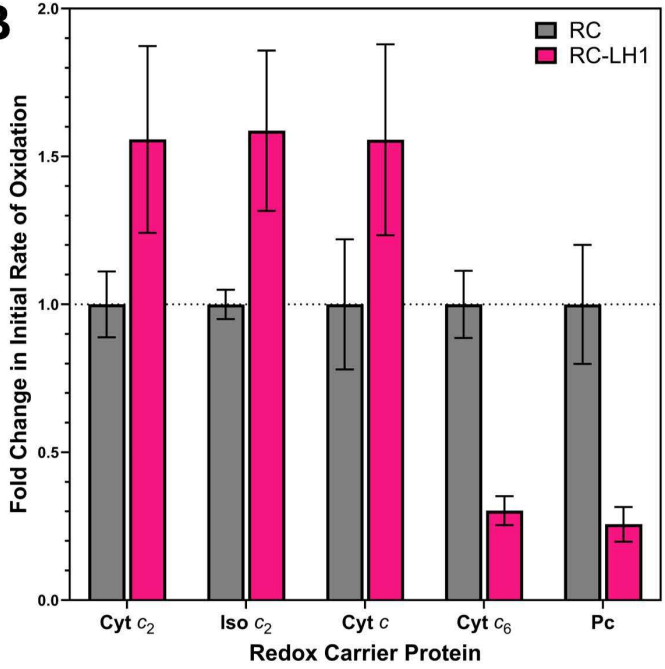

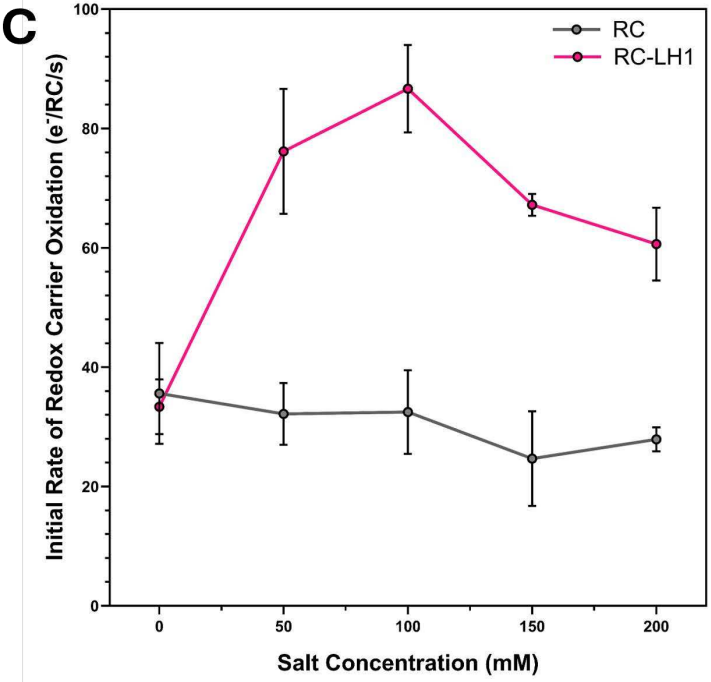

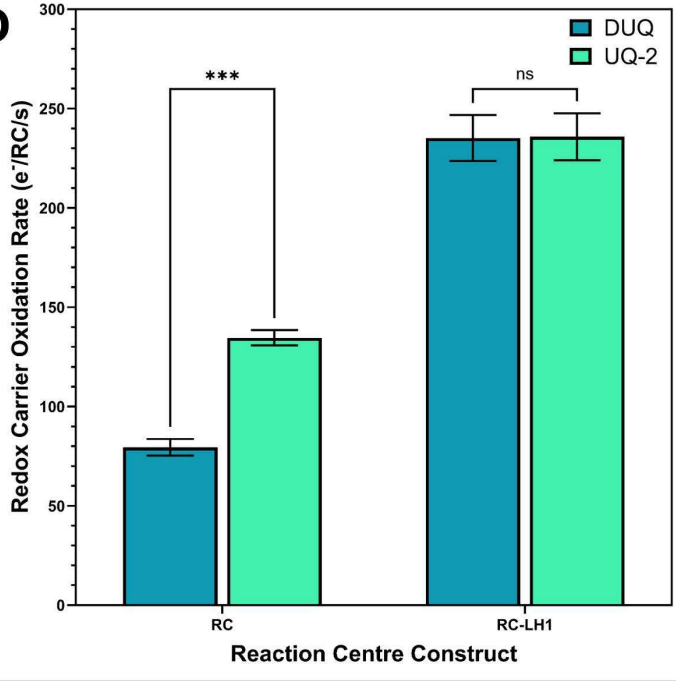

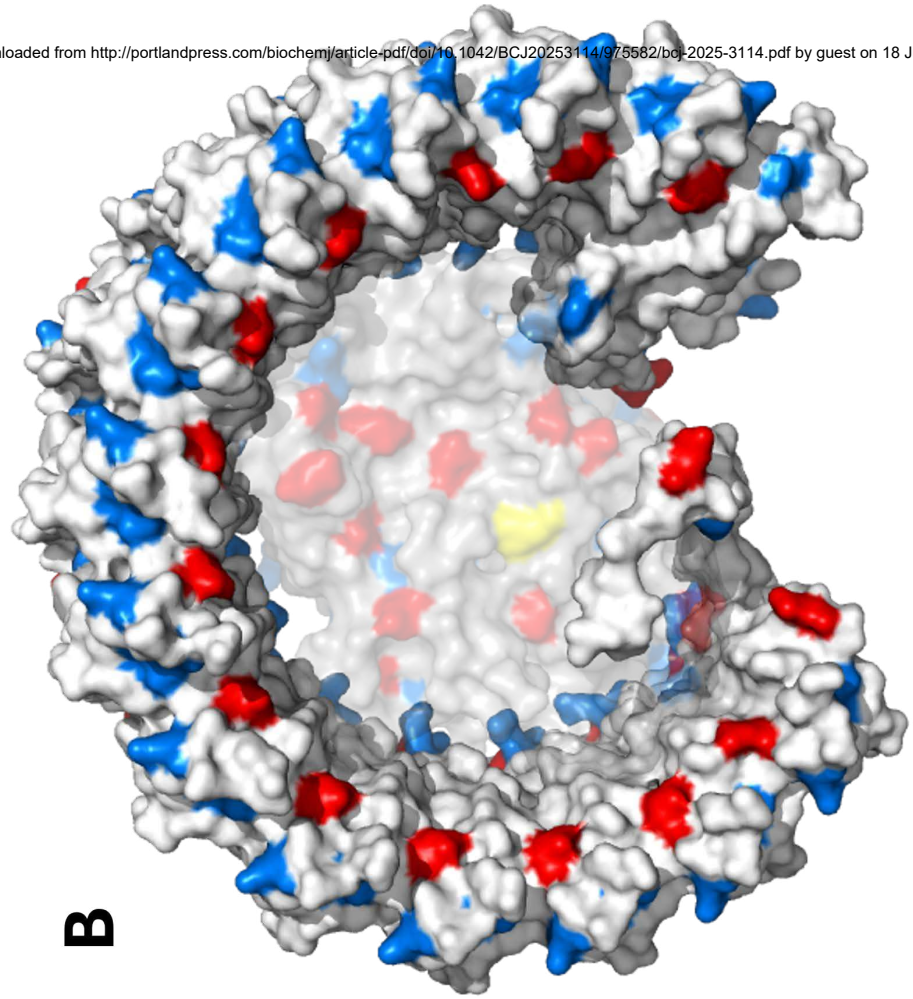

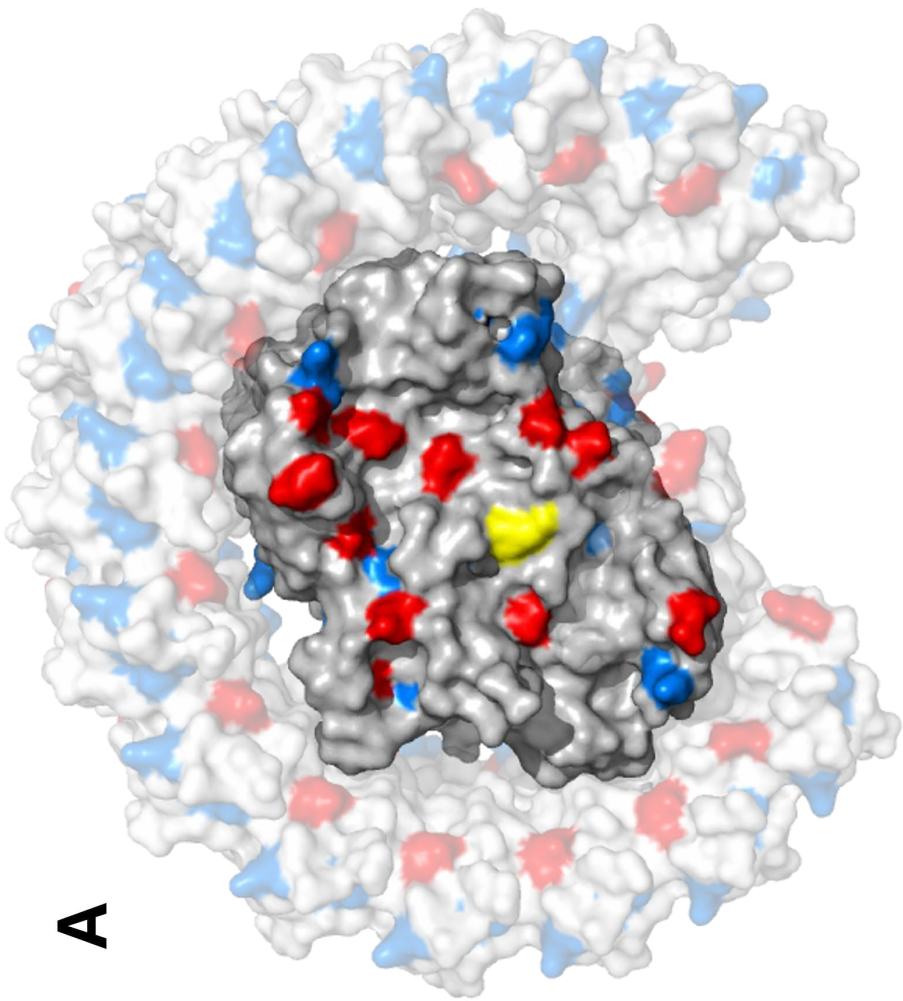

	Cyt c_2	Iso c_2	Cyt c_6	Pc
Edge-to-Edge Distance (Å)	8.1	8.0	7.9	13.1
HADDOCK Score	-183	-144	-104	-91.9
Predicted k_{et} (s^{-1})	1.38×10^9	7.53×10^9	3.23×10^9	2.77×10^5
Doubling Time (hours)	9.15	9.69	10.3	36.1
V_{max} (e^-/RC/s)	293	230	37.8	7.92
K_M (µM)	6.80	5.88	66.3	209
Optimum [NaCl] (mM)	100	50	700	700

Table 2: Bacterial strains used in this study

Species/strain	Genotype	Properties	Source/Reference
***Rhodobacter sphaeroides* 2.4.1**			
Wild type	N/A	Wild type strain	S. Kaplan (University of Texas)
Δ*cycA* Δ*cycI*	Δ*cycA* Δ*cycI*	Unmarked deletion of *cycA* (RSP_0296) and *cycI* (RSP_2577); does not produce cyt c_2 (*cycA*) or iso c_2 (*cycI*)	[53]
DX13	Δ*puc1BA* Δ*puc2BA* PufX R49L R53L	Unmarked deletion strain of LH2 genes, *puc1BA* (RSP_0314-0315) and *puc2BA* (RSP_1556-1557). Replacement of arginine residues in PufX responsible for dimerization with leucine so strain exclusively makes RC-LH1 monomers.	This study S. Kaplan (University of Texas) (Δ*puc1BA*) [78] (Δ*puc2BA*) [79] (PufX R49L R53L)
E9	Δ*puc1BA* Δ*pufBALM*	Unmarked deletion strain of LH2 genes, *puc1BA* (RSP_0314-0315), along with *pufBALM* (RSP_6108, RSP_0258-0256) encoding the RC-LH1 l, M, α and β subunits.	This study S. Kaplan (University of Texas) (Δ*puc1BA*)
Escherichia coli			

BL21(DE3)	F– *ompT hsdSB* (r_B^-, m_B^-) *gal dcm* (DE3)	Protein production strain	Promega
JM109	*end*A1, *rec*A1, *gyr*A96, *thi*, *hsd*R17 (r_k^-, m_k^+), *rel*A1, *sup*E44, Δ(*lac-proAB*), [F´ *tra*D36, *pro*AB, *laq*I^{q}Z ΔM15]	Cloning strain	Promega
S17-1	RP4-2 (Tc::Mu, Nm::Tm7) integrated into the chromosome *Tp*^{R} *Sm*^{R} *rec*A, *thi*, *pro*, *hsd*M$^+$	Conjugative transfer of plasmids to *Rba. sphaeroides*	[80]
Synechocystis	**sp. PCC 6803**		
Wild type	N/A	Glucose-tolerant wild-type strain	R. Sobotka (Algatech, Třeboň)

Table 3: Extinction coefficients used in this study

Species	Wavelength	Extinction Coefficient, ε (mM^{-1})	Source
RC-LH1	875	3000	[84]
RC	802	288	[85]
Cyt c_2	550	30.8 (reduced) 21.5 (reduced – oxidised)	[20]
Iso c_2	551	25.6 (reduced) 19.1 (reduced – oxidised)	This study
Cyt c_6	552	24.1 (reduced) 19.5 (reduced-oxidised)	[43] [86]
Pc	597	4.5 (reduced) 4.5 (reduced-oxidised)	[87]
Cyt c	550	27.6 (reduced) 21.1 (reduced – oxidised)	[88]
DUQ	278	14 (oxidised in EtOH	[89]
UQ-2	275	13.7 (oxidised in EtOH)	[89]

Supporting Information for:

Cyanobacterial redox carriers support photosynthesis in a purple phototrophic bacterium

Adam G.M. Bowie[1], Andrew Hitchcock[1,2*], Matthew S. Proctor[1], Elizabeth C. Martin[1], David J.K. Swainsbury[3] and C. Neil Hunter[1*]

[1]Plants, Photosynthesis and Soil, School of Biosciences, University of Sheffield, UK.

[2]Molecular Microbiology: Biochemistry to Disease, School of Biosciences, University of Sheffield, UK.

[3]School of Biological Sciences, University of East Anglia, Norwich Research Park, Norwich, UK.

*Correspondence: C. Neil Hunter (c.n.hunter@sheffield.ac.uk); Andrew Hitchcock (a.hitchcock@sheffield.ac.uk)

Author ORCID IDs: 0009-0008-6246-4544 (AGMB), 0000-0001-6572-434X (AH), 0000-0002-1484-850X (MSP), 0000-0001-9600-7298 (ECM), 0000-0002-0754-0363 (DJKS), 0000-0003-2533-9783 (CNH).

Table of Contents

Supplementary Table 1	Primers used in this study	**Page 2**
Supplementary Table 2	Predicted electron transfer rates from redox carrier proteins to RC-LH1 and PSI complexes	**Page 3**
Supplementary Figure 1	Predicted protein-protein docking affinities by the HADDOCK 2.4 server	**Page 4**
Supplementary Figure 2	Effect of pH on the initial rate of Cyt c_2 oxidation by the WT RC-LH1 core complex	**Page 5**
Supplementary Figure 3	Raw data showing the effect of increasing NaCl Concentration on initial rates of redox carrier oxidation by RC-LH1 Complexes	**Page 6**
Supplementary Figure 4	Light saturation of RC and RC-LH1 complexes in steady state turnover	**Page 7**

	assays with cyt c_2	
Supplementary Figure 5	Coomassie-stained SDS-PAGE gel of all purified redox carrier proteins	**Page 8**
Supplementary Figure 6	Steady-state oxidation rates of untagged and StrepII-tagged Pc isoforms by RC-only complexes	**Page 9**

Supplementary Table 1.

Name	5'-3' Sequence	Sites
pufBALM KO UF	CCG**GAATTC**GAGAGGGTCGTGAGAGAGACTG	EcoRI
pufBALM KO UR	GCGC**TCTAGA**AGCCATGCTATCCTCCGGATCG	XbaI
pufBALM KO DF	GCGC**TCTAGA**AACTGAGGAGCGATCACAATG	XbaI
pufBALM KO DR	CCCC**AAGCTT**GCAGCAGACGCGATCCAAAAG	HindIII
pufBALM Scr F	GCCCTGGACCGCATCGTAGAGG	
pufBALM Scr R	CGAAATCACCTCGGAACGCACT	
cycI KO Scr Fwd	CATTTCGTGAATCCGTCCGAGATCG	
cycI KO Up Fwd	CCG**GAATTC**CAACGTGAAGGTGATGCGTCAGG	EcoRI
cycI KO Up Rev	CATTTCAGCCCTCCAATCTCATGGTCTTCTCCCTTTGCG	
cycI KO Down Fwd	CTG**AAGCTT**GCCCACGTTCTCG	HindIII
cycI KO Scr Rev	GCCACAGGATCTTGCCGTCATTG	
cycA Fwd	AGCT**AGATCT**ATGAAGTTCCAAGTCAAGG	BglII
cycA Rev	TGAC**CTCGAG**TCAGGGCCGGACGGCGA	XhoI
cycI Fwd	AGCT**AGATCT**ATGAGATTGACCACCATCC	BglII
cycI Rev	TGAC**GTCGAC**TCAGCCCTCCGCCGGCG	SalI
petJ (Syn) Fwd	AGCT**AGATCT**ATGTTTAAATTATTCAACCAAGCTAGC	BglII
petJ (Syn) Rev	TGAC**CTCGAG**CTACCAGCCCTTTTCCGC	XhoI
petJ (Thermo) Fwd	CGC**GGATCC**ATGAAAAAGCGATTCATTAG	BamHI
petJ (Thermo) Rev	TGAT**CTCGAG**TTAGCCTGCCCAACCCTTG	XhoI
petE Fwd	AGCT**AGATCT**ATGTCTAAAAAGTTTTTAACAATCCTCG	BglII

petE Rev	TGAC**CTCGAG**TTACTCAACGACAACTTTGCCTA	XhoI
petE-StrepII Fwd	AATTAA**CCATGG**GCTCCAAGAAGTTTTTGACAATTTTAGCGG	NcoI
petE-StrepII Rev	AGCAAT**CTCGAG**CTACTTCTCAAATTGGGGGTGACTCCACGCCGA	XhoI

Primers used in this study. Restriction sites used for cloning are underlined in bold.

Supplementary Table 2.

Electron Donor	Electron Acceptor	Distance (Å)	ΔG (eV)	λ (eV)	k_{et} (s^{-1})
Cyt c_2	RC-LH1	8.1	-0.115	0.500	2.40×10^9
Iso c_2	RC-LH1	8.0	-0.173	0.500	4.98×10^9
Cyt c_6	RC-LH1	7.9	-0.143	0.500	4.26×10^9
Pc	RC-LH1	13.1	-0.107	0.500	2.18×10^6
Cyt c_6	PSI	10.4	-0.130	0.418	2.02×10^8
Pc	PSI	14.3	-0.094	0.418	6.31×10^5

Predicted electron transfer rates from redox carrier proteins to RC-LH1 and PSI complexes. *Calculations were made using the following equation (Moser et al., 2010), where R is the electron transfer distance in angstroms (Å), ΔG is the free energy change in electron volts (eV) and λ is the reorganisation energy, also in eV.*

$$log_{10}k_{et}^{ex} = 13 - 0.6(R - 3.6) - 3.1(\Delta G + \lambda)^2/\lambda$$

Electron transfer distances represent edge-to-edge cofactor distances and were calculated from AlphaFold3 models (Abramson et al., 2024), whilst ΔG values were computed from midpoint redox potentials for P_{865}/P_{865}^+ (Visschers et al., 1999), P_{703}/P_{703}^+ (Nakamura et al., 2011), cyt c_2/cyt c_2^+ (Pettigrew et al., 1976), iso c_2/iso c_2^+ (Rott et al., 1992), cyt c_6/cyt c_6^+ and Pc/Pc^+ (Diaz et al., 1994). Reorganisation energies of +0.5 eV and +0.418 eV were used for electron transfers to RC-LH1 (Lin et al., 1994) and PSI (Caspy et al., 2021), respectively.

Supplementary Figure 1.

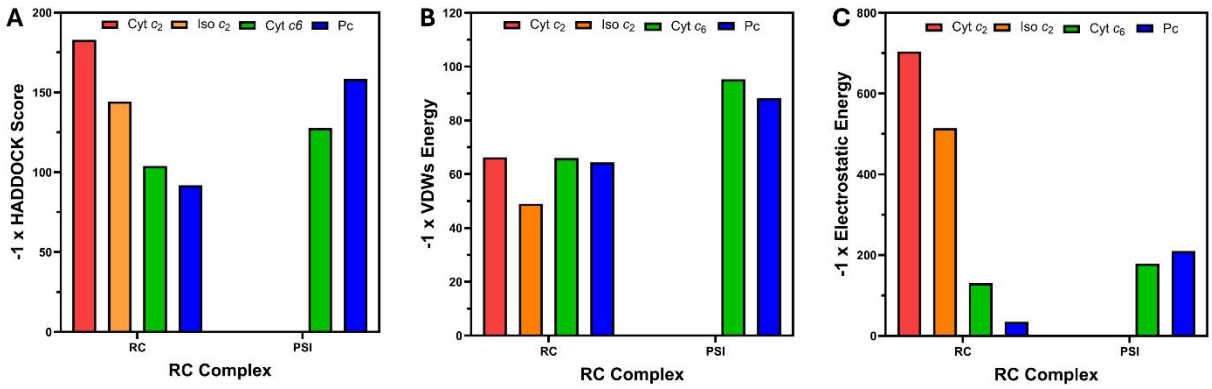

Predicted protein-protein docking affinities by the HADDOCK 2.4 server. Bar charts of **(A)** Haddock scores, **(B)** van der Waals (VDW) energies and **(C)** electrostatic energies of the native and non-native RC-redox carrier complexes, calculating using the HADDOCK 2.4 server running v2.4-2022.08 (Honorato et al., 2024). For simplicity, all values displayed in the bar charts have been transformed from negative to positive values by multiplying by -1. The output of the HADDOCK 2.4 docking tool is a "HADDOCK score", which is a weighted sum of the contributing energy components, including VDW forces, electrostatic interactions, desolvation energies and restraint violation energies. This headline score is a model of free energy (ΔG) but is not directly comparable to experimentally determined values.

Supplementary Figure 2.

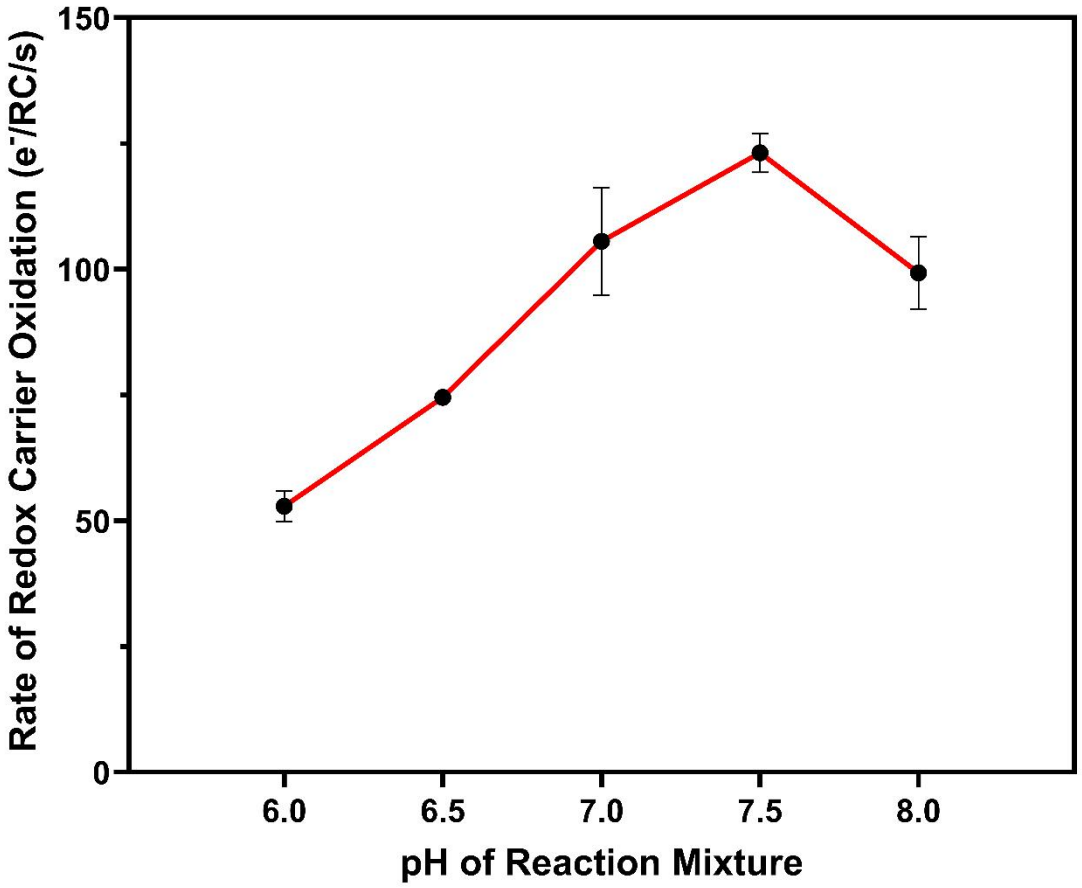

Effect of pH on the initial rate of cyt c_2 oxidation by the WT RC-LH1 core complex. To determine the optimum pH value for the RC-LH1 cyt c_2 system, a set of steady-state turnover assays were conducted in triplicate over a range of buffer conditions between pH 6 and 8. Each reaction mixture contained 0.5 µM RC-LH1, 10 µM cyt c2, 500 µM DUQ, 200 mM NaCl, 0.03 % w/v and 100 mM of either Bis-Tris (pH 6 – 6.5), HEPES (pH 7 – 7.5) or Tris-HCl (pH 8) buffers.

Supplementary Figure 3.

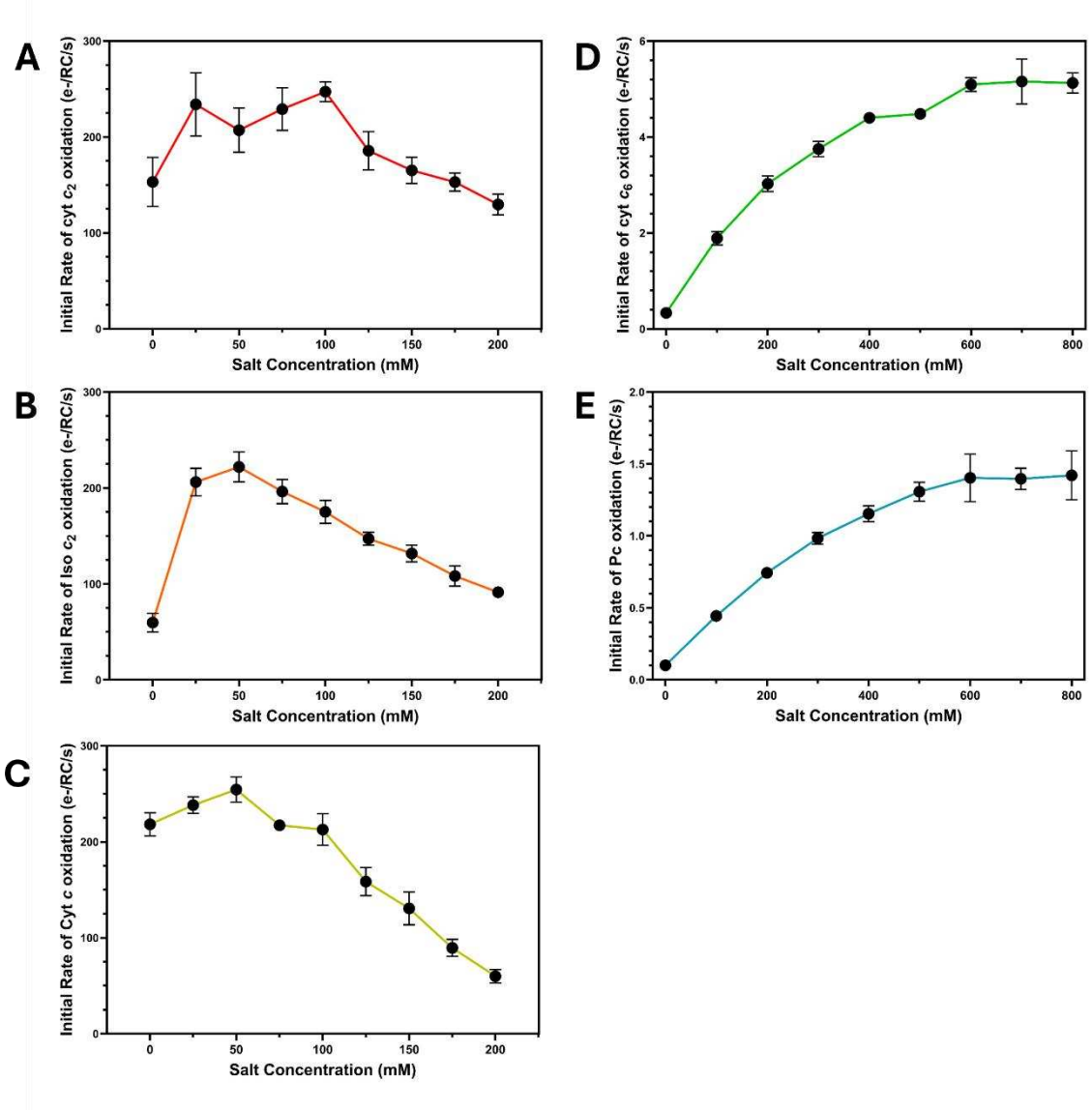

Raw data showing the effect of increasing NaCl Concentration on initial rates of redox carrier oxidation by RC-LH1 Complexes. Salt dependency of the interaction between RC-LH1 and **(A)** cyt c2 from Rba. sphaeroides, **(B)** iso c2 from Rba. sphaeroides, **(C)** cyt c from Equus caballus, **(D)** cyt c6 from Synechocystis sp. PCC 6803 and **(E)** Pc from Synechocystis sp. PCC 6803. These graphs show the raw turnover rates that are also presented in Figure 6 of the main text, with error bars showing mean and standard deviation.

Supplementary Figure 4.

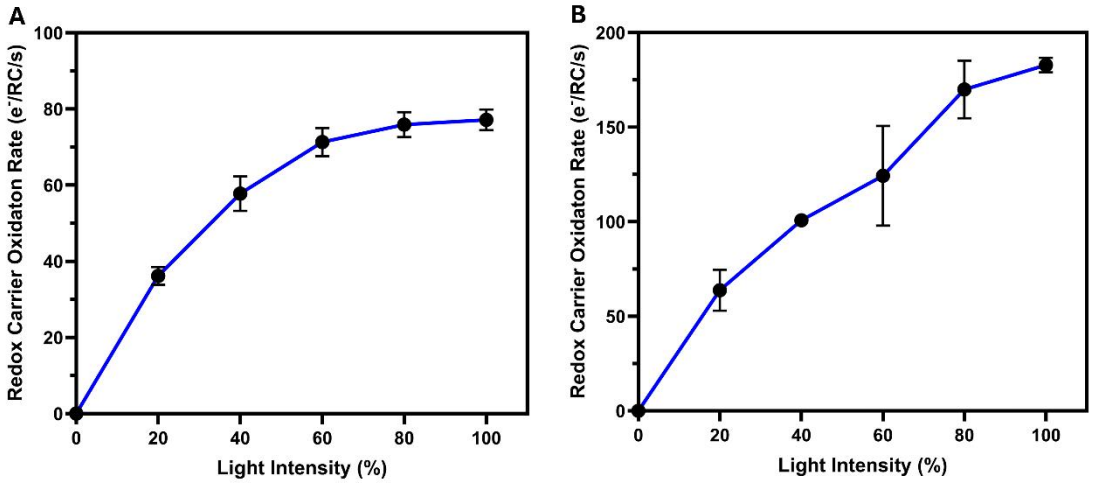

Light saturation of RC and RC-LH1 complexes by 810 nm LED in steady state turnover assays with cyt c_2. RC and RC-LH1 complexes were assayed in slightly different reaction mixtures, but both under the same conditions of 50 mM Tris-HCl buffer pH 7.5 with 100 mM NaCl and 0.03 % w/v β-DDM. **(A)** Cyt c_2 oxidation rate in reaction mixtures containing 0.5 µM RC, 10 µM cyt c_2 and 500 µM DUQ. **(B)** Cyt c_2 oxidation rate in reaction mixtures containing 0.5 µM RC-LH1, 1 mM sodium ascorbate, 10 µM cyt c_2 and 50 µM UQ-2. The results clearly show that at 100 % intensity, the red-light pulse is saturating for the RC-only complex, and despite greater experimental noise, saturating or nearly saturating for RC-LH1. Therefore, it can be assumed that any observed oxidation rate differences are not caused the greater light harvesting activity of the physiological complex.

Supplementary Figure 5.

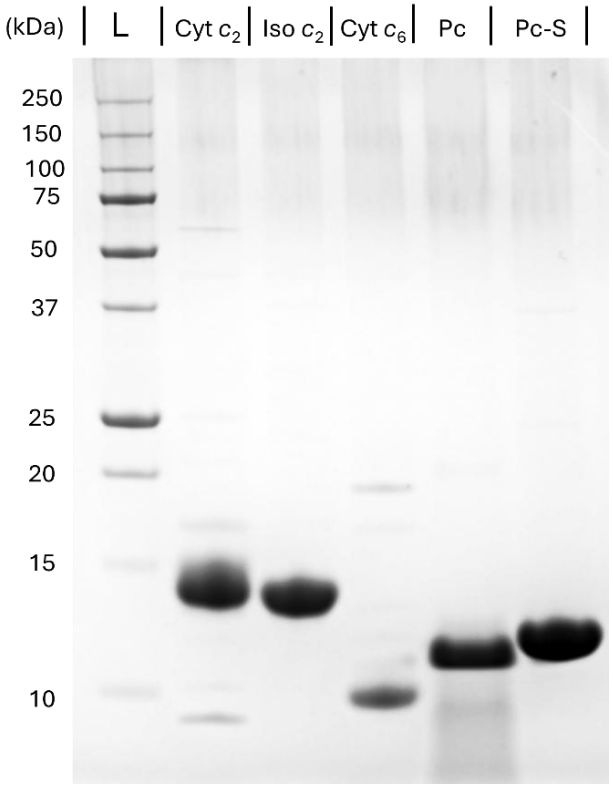

Coomassie-stained SDS-PAGE gel of all purified redox carrier proteins. From left to right, cyt c_2 (13.5 kDa) from *Rba. sphaeroides*, iso c_2 (12.9 kDa) from *Rba. sphaeroides*, cyt c_6 (8.7 kDa) from *Rba. sphaeroides*, Pc (10.3 kDa) from *Rba. sphaeroides* and Strep-tagged Pc (11.5 kDa) from *E. coli*.

Supplementary Figure 6.

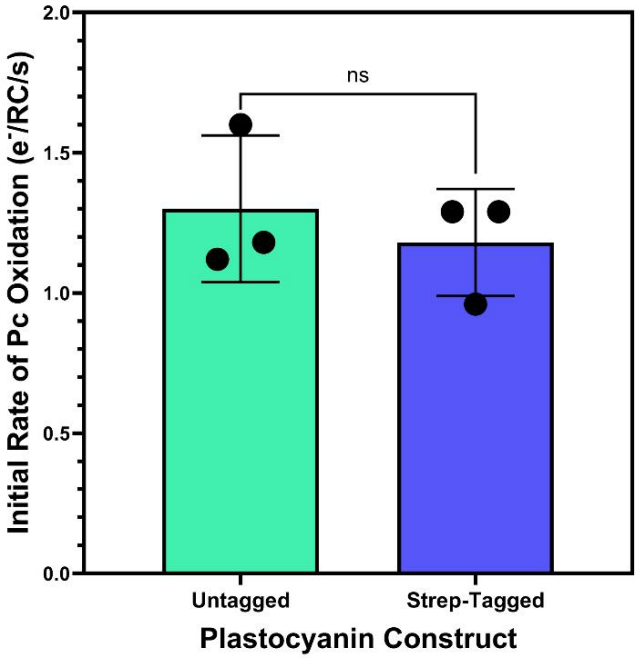

Steady-state oxidation rates of untagged and StrepII-tagged Pc isoforms by RC-only complexes. *To test if the presence of the StrepII tag made any difference to the oxidation kinetics, steady-state turnover assays were conducted using both tagged and untagged isoforms of the protein in reaction mixtures containing 0.125 µM RC, 10 µM Pc and 50 µM UQ-2 in turnover buffer (50 mM Tris pH 7.5, 100 mM NaCl and 0.03 % (w/v) β-DDM). These assays conclusively showed no difference between the two versions of Pc, with overlapping error bars and a p-value of 0.56 (ns) obtained using an unpaired t test with Welch's correction applied.*